Ⓔ

Revising Estimates of Spatially Variable Subsidence during the A.D. 1700 Cascadia Earthquake Using a Bayesian Foraminiferal Transfer Function

by Andrew C. Kemp, Niamh Cahill, Simon E. Engelhart, Andrea D. Hawkes, and Kelin Wang

Abstract Coseismic subsidence along the Cascadia subduction zone causes abrupt relative sea-level (RSL) rise that is recorded in coastal stratigraphy and foraminiferal assemblages. RSL reconstructions therefore provide insight into the magnitude, nature, and frequency of great earthquakes that can constrain deformation models and quantify the seismic risk faced by coastal populations. These reconstructions are commonly generated using transfer functions that are calibrated from counts of modern (surface) foraminifera and corresponding elevation measurements. We developed four transfer functions of increasing complexity to explore how and why the composition of the modern dataset and the choice of transfer-function type affects subsidence reconstructions. Application of these four models to stratigraphic contacts (mud abruptly overlying peat or soil) representing the A.D. 1700 Cascadia earthquake and a field experiment that simulated subsidence show that a Bayesian transfer function (BTF) calibrated using a large modern dataset (19 sites from California to Vancouver Island) and incorporating prior information from stratigraphic context produces systematically larger subsidence estimates than a weighted-averaging transfer function calibrated using a smaller modern dataset (8 sites in Oregon) that does not leverage stratigraphic context. This difference arises from (1) training set composition, (2) taxa–elevation relationships in the BTF that are not assumed to be unimodal, and (3) stratigraphic prior information that compensates for postdepositional, downward mixing of postearthquake foraminifera into pre-earthquake sediment, which biases reconstructions at some sites toward smaller subsidence. Our reconstructions support a heterogeneous rupture model for the A.D. 1700 earthquake, but indicate that slip estimates in patches from Alsea Bay to Netarts Bay (Oregon) and from Netarts Bay to Vancouver Island should be increased.

Electronic Supplement: Table listing counts of foraminifera and sample elevations used to construct the West Coast modern training set.

Introduction

During the Holocene, repeated great ($M_w > 8.0$) earthquakes along the Cascadia subduction zone (Fig. 1) produced a cyclical pattern of vertical land motion that is recorded in tidal wetland stratigraphy as relative sea-level (RSL) change (e.g., Atwater, 1987, 1992; Nelson, 1992; Darienzo *et al.*, 1994; Nelson *et al.*, 1996; Shennan *et al.*, 1996; Atwater and Hemphill-Haley, 1997; Kelsey *et al.*, 2002; Witter *et al.*, 2003; Atwater *et al.*, 2005). During the interseismic phase (100–1000 s of years) of Cascadia's earthquake deformation cycle, strain accumulation on the plate boundary causes coastal uplift (RSL fall). This strain is then released during the seconds-to-

minutes-long coseismic phase when the coast subsides (RSL rise). Establishing the timing and geographic pattern of coseismic deformation using RSL reconstructions therefore provides insight into subduction deformation processes and the history (magnitude and recurrence interval) of earthquakes along the Cascadia subduction zone (e.g., Witter *et al.*, 2003; Nelson *et al.*, 2006; Leonard *et al.*, 2010; Hawkes *et al.*, 2011; Wang *et al.*, 2013; Milker *et al.*, 2016; Hutchinson and Clague, 2017). RSL reconstructions are generated using proxies such as plants and assemblages of foraminifera, diatoms, and/or pollen that are preserved in coastal sediment and have a

654

consistent and quantifiable relationship to tidal elevation (e.g., Hemphill-Haley, 1995; Shennan *et al.*, 1996; Hughes *et al.*, 2002; Hawkes *et al.*, 2010).

Salt-marsh foraminifera are widely used proxies for reconstructing earthquake-driven RSL change along the Pacific coast of North America because they display a strong relationship to tidal elevation (e.g., Jennings and Nelson, 1992; Scott *et al.*, 1996; Hawkes *et al.*, 2010), respond rapidly to environmental change (e.g., Engelhart, Horton, Nelson, *et al.*, 2013; Horton *et al.*, 2017), and form low-diversity assemblages that are commonly composed of many hundreds of individuals, which makes them well suited to quantitative analysis (e.g., Edwards and Wright, 2015). Efforts to accurately and precisely quantify coastal subsidence often rely on transfer functions (e.g., Guilbault *et al.*, 1996; Hawkes *et al.*, 2011; Milker *et al.*, 2016) that are empirically derived and regression-based equations for quantifying past environmental conditions from paleontological data (Sachs *et al.*, 1977). The most commonly used transfer functions for reconstructing RSL utilize weighted averaging (WA) methods (e.g., Barlow *et al.*, 2013; Kemp and Telford, 2015), in which all species are assumed to have a unimodal relationship to the environmental variable of interest (e.g., Birks, 1995; Juggins and Birks, 2012). This relationship is established empirically using a modern training set of paired observations of species abundance in surface sediment and accompanying measurements of tidal elevation. Recently developed Bayesian transfer functions (BTFs) offer an alternative approach to WA transfer functions that allows for flexible species-response curves (including nonunimodal forms) and can formally incorporate prior information from additional proxies (e.g., counts of another microfossil group, $\delta^{13}C$ measurements, or stratigraphic context) to further improve accuracy and precision (Cahill *et al.*, 2016; Holden *et al.*, 2017). Variability in the composition of foraminiferal assemblages among sites and regions means that it is often necessary to construct a sufficiently diverse and geographically widespread modern training set to provide modern analogs for assemblages that are likely to be encountered in the stratigraphic record (e.g., Horton and Edwards, 2005; Watcham *et al.*, 2013; Shennan *et al.*, 2016).

Comparison of coseismic subsidence reconstructed from proxies and predicted by deformation models (e.g., Leonard *et al.*, 2004, 2010; Wang *et al.*, 2013) facilitates the development and refinement of models to better characterize seismic risk for coastal populations living along the Cascadia subduction zone. Therefore, it is important that deformation models are compared with accurate and precise coseismic subsidence reconstructions. To explore how and why the choice of training set and transfer-function type influences the amount and geographic pattern of reconstructed coseismic subsidence, we re-estimated coastal subsidence during the A.D. 1700 earthquake at 13 sites along the Cascadia subduction zone using four transfer functions of increasing complexity. The four models were a WA transfer function calibrated using a modern dataset of 169 samples from eight sites in Oregon (similar to the transfer function used by Milker *et al.*,
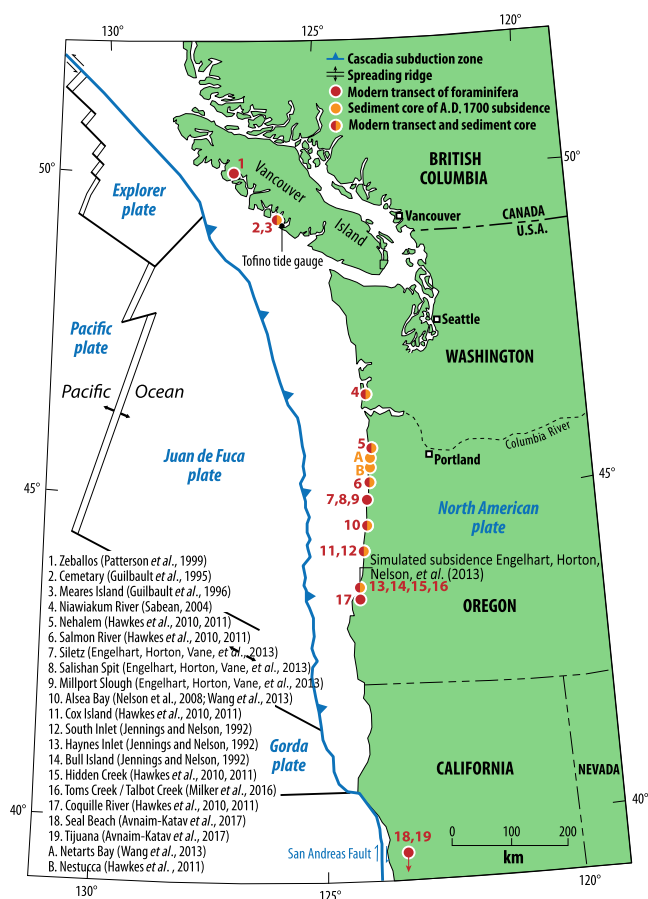

Figure 1. Location of sites used in this study along the Pacific coast of North America. In some instances, more than one site is represented by a symbol because of their close proximity. The West Coast training set is composed of modern data from 19 sites. The A.D. 1700 earthquake is recorded in the stratigraphic record at 13 sites (with two independent reconstructions at the Alsea Bay site in Oregon). A marsh transplant study performed at Hidden Creek in South Slough, Oregon, by Engelhart, Horton, Nelson, *et al.* (2013) simulated coseismic subsidence. Modified from Atwater (1992) and Hawkes *et al.* (2010). The color version of this figure is available only in the electronic edition.

2016), a second WA transfer function calibrated with an expanded modern dataset composed of 393 samples from 19 sites between southern California and Vancouver Island and two BTFs calibrated with the expanded modern dataset. One BTF used no additional information (uninformative priors), and the other incorporated information from stratigraphic context (informative priors). Sequential comparison of reconstructions from these four transfer functions allowed us to demonstrate how and why coseismic subsidence reconstructions are influenced by (1) expansion of the modern training set to span the length of the Cascadia subduction zone (as opposed to existing subregional datasets); (2) allowing species to have nonunimodal relationships to elevation (as opposed to the widespread assumption of a unimodal form for all species), including where along the Cascadia subduction zone species with nonunimodal distributions are more or less likely to be

encountered in the stratigraphic record; and (3) formal incorporation of independent and informative priors (as opposed to existing studies that use a single proxy or utilize secondary information informally).

Tectonic Setting, Glacio-Isostatic Adjustment, and Tidal-Marsh Zonation

Along the Cascadia subduction zone, three remnants of the Farallon plate (Gorda, Juan de Fuca, Explorer) are subducted beneath the North American plate (Fig. 1) at 30–42 mm/yr (DeMets *et al.*, 2010). The megathrust is currently locked to some degree, resulting in margin-normal shortening and fore-arc uplift (e.g., Wang *et al.*, 2012; McCaffrey *et al.*, 2013; Schmalzle *et al.*, 2014). Although the exact degree of locking is not observationally constrained, full locking is commonly assumed for most of the margin, based on thermal arguments and the extraordinarily low interplate seismicity at present (Wang and Tréhu, 2016). The Pacific coast of North America experiences ongoing glacio-isostatic adjustment that drives long-term (multimillennial) and spatially variable RSL trends. During the late Holocene, this process caused RSL fall at locations north of Washington, which is not conducive to preservation of multiple earthquakes through time (Nelson, 2013; Engelhart *et al.*, 2015; Dura, Engelhart, *et al.*, 2016). This is one reason why the A.D. 1700 earthquake is more intensively studied than older events that occurred along the Cascadia subduction zone.

Cascadia's tidal marshes are composed of expansive tidal flats sequentially replaced at higher elevations by low salt-marsh, high salt-marsh, and freshwater upland environments that host distinctive plant communities and are characterized by deposition of different sediment types (e.g., Redfield, 1965; Seliskar and Gallagher, 1983; Nelson and Kashima, 1993; Peterson *et al.*, 2000; Witter *et al.*, 2003; Hawkes *et al.*, 2010; Milker *et al.*, 2016). In low salt-marsh and tidal-flat environments below mean high water (MHW), surface sedimentation is dominated by marine silt and clay with little or no *in situ* organic material. Peat formation in high salt-marsh environments above mean higher high water (MHHW) results in organic-rich sediment with a fibrous texture and the inclusion of *in situ* and identifiable remains of vascular plants. Freshwater, upland environments above the influence of tides are characterized by soil formation. In the stratigraphic record preserved beneath modern tidal marshes, these different environments are readily recognized and distinguished from one another through the qualitative (e.g., field descriptions) and quantitative (e.g., loss-on-ignition measurements and identification of plant macrofossils) characteristics of sedimentary units.

Datasets

Standardization of Modern Training Sets

All transfer functions require calibration using a training set to quantify the modern (observable) relationship between foraminifera and tidal elevation. Modern training sets are composed of counts of foraminifera in surface sediment where the elevation of the sample was measured relative to local tidal datums at the time of collection. A point of ongoing debate in the sea-level research community is what the geographic and ecological scope of a modern training set should be (e.g., Watcham *et al.*, 2013). Larger and more diverse training sets typically provide a broader suite of modern analogs and capture a greater degree of natural variability in taxa–elevation relationships than smaller, localized training sets, but these advantages often come at the expense of reduced precision (e.g., Horton and Edwards, 2005). Several datasets relating modern foraminifera to tidal elevation are available from tidal marshes along the Pacific coast of North America, and we compiled and standardized modern data from 19 sites (Table 1; Fig. 2) to develop a large and diverse training set that could be applied to fossil assemblages from an equally diverse set of paleoenvironments.

To combine samples from sites with different tidal ranges, elevation is expressed as a standardized water-level index (SWLI) rather than as an absolute value in meters relative to (for example) mean tide level (MTL; e.g., Horton and Edwards, 2006). We expressed elevation as an SWLI in which a value of 100 equates to local MTL and a value of 200 is local MHHW. For datasets from the United States, absolute sample elevations are expressed relative to tidal datums defined by the National Oceanic and Atmospheric Administration (NOAA). These tidal datums are calculated from observed water levels over the 1983–2001 tidal epoch. We also included modern datasets from Vancouver Island, Canada, where different tidal datums are defined from water-level predictions rather than observations. For consistency among datasets, we calculated tidal datums using NOAA definitions for Meares Island and Cemetery (Guilbault *et al.*, 1995, 1996) from hourly water-level measurements made by the Tofino tide gauge (Fig. 1) from 1 January 1983 to 31 December 2001. We assumed that the equivalence between NOAA and Canadian tidal datums observed at Tofino was also appropriate for the modern dataset from Zeballos (Patterson *et al.*, 1999; Fig. 1). The datum for reported sample elevations at Cemetery and Meares Island was the lower edge of the freshwater forest (Guilbault *et al.*, 1995, 1996), which we treated as equivalent to the height reached only by the highest 1% of high tides at Tofino. This elevation is the same as the reported elevation of highest astronomical tide at Tofino.

We took several steps to standardize taxonomy when combining counts of foraminifera from multiple studies. All species of *Haplophragmoides* were combined into a single group. In the datasets from Meares Island and Cemetery, counts of *Jadammina macrescens* var. *polystoma* were treated as *Jadammina macrescens* in the combined dataset, whereas *Jadammina macrescens* was standardized as *Balticammina pseudomacrescens* following discussions with the author that originally produced the data (Guilbault *et al.*, 1995, 1996). All species of calcareous foraminifera were combined into a single group. All species of *Ammobaculites*
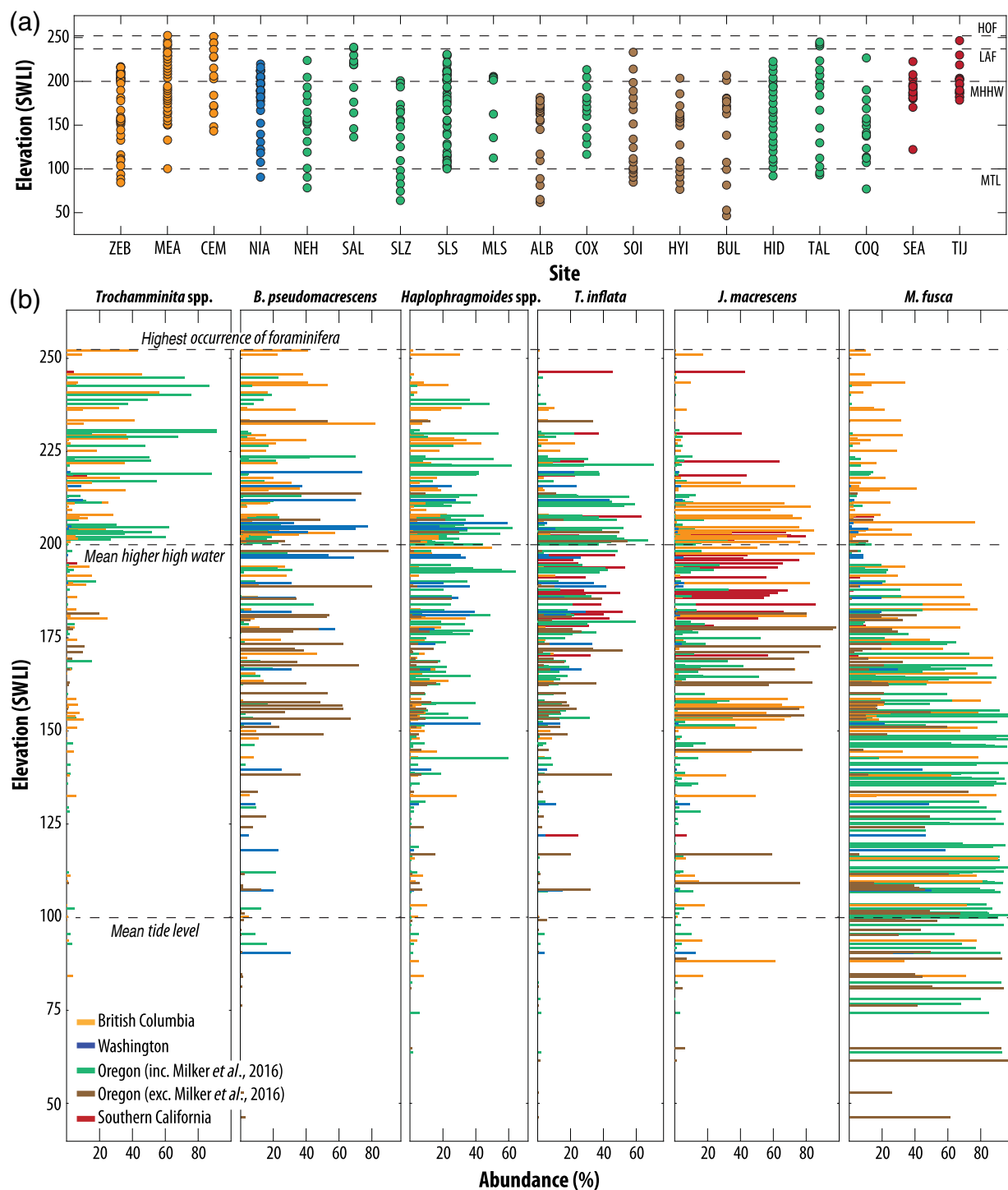
Figure 2. Compiled modern training set of salt-marsh foraminifera from 19 sites along the Pacific coast of North America. Only samples with counts greater than 30 foraminifera are presented. (a) Distribution of samples by elevation at each site (ordered approximately from north to south). ZEB, Zeballos; CEM, Cemetery; MEA, Meares Island; NIA, Niawiakum; NEH, Nehalem; SAL, Salmon River; SLZ, Siletz East; SLS, Salishan Spit; MLS, Millport Slough; ALB, Alsea Bay; COX, Cox Island; SOI, South Inlet; HYI, Haynes Inlet; BUL, Bull Island; HID, Hidden Creek; TAL, Talbot Creek; COQ, Coquille; SEA, Seal Beach; TIJ, Tijuana. (b) Assemblages of foraminifera expressed as percentages. Only the seven most abundant species are presented. Together, these species represent ~94% of the ~125,000 individual foraminifera in the standardized modern dataset. In both panels, sample elevation is expressed as a standardized water-level index (SWLI), in whch a value of 100 corresponds to local mean tide level (MTL), and a value of 200 corresponds to local mean higher high water (MHHW). The highest occurrence of foraminifera (HOF) across the entire dataset is found at 252 SWLI; the lowest sample in which foraminifera were absent (LAF) occurred at 236 SWLI. Symbol and bar shading represents the state or province from which the samples were collected. Samples from Oregon are further divided to represent sites used and not used in the transfer function of Milker *et al.* (2016). The color version of this figure is available only in the electronic edition.

Table 1
Data Used in the Regional-Scale Modern Training Sets

Site	References	Range (SWLI)	N	Type
Alsea Bay (OR)	Nelson *et al.* (2008)	61–181	18	Dead, 0–2 cm
Bull Island (OR)	Jennings and Nelson (1992)	46–207	15	Total, 0–1.5 cm
Cemetery (BC)	Guilbault *et al.* (1995)	143–251	15	Dead, 0–2 cm
Cox Island (OR)*	Hawkes *et al.* (2010)	116–213	12	Dead, 0–1 cm
Coquille River (OR)*	Hawkes *et al.* (2010)	77–227	15	Dead, 0–1 cm
Haynes Inlet (OR)	Jennings and Nelson (1992)	76–203	19	Total, 0–1.5 cm
Hidden Creek (OR)*	Hawkes *et al.* (2010)	92–223	23	Dead, 0–1 cm
Meares Island (BC)	Guilbault *et al.* (1996)	100–252	33	Dead, 0–2 cm
Millport Slough (OR)*	Engelhart, Horton, Vane, *et al.* (2013)	112–205	9	Dead, 0–1 cm
Niawiakum River (WA)	Sabean (2004)	90–220	34	Total, 0–1 cm
Nehalem River (OR)*	Hawkes *et al.* (2010)	78–224	16	Dead, 0–1 cm
Siletz East (OR)*	Engelhart, Horton, Vane, *et al.* (2013)	64–200	17	Dead, 0–1 cm
South Inlet (OR)	Jennings and Nelson (1992)	85–233	17	Total, 0–1.5 cm
Salmon River (OR)*	Hawkes *et al.* (2010)	136–244	14	Dead, 0–1 cm
Salishan Spit (OR)*	Engelhart, Horton, Vane, *et al.* (2013)	100–231	48	Dead, 0–1 cm
Seal Beach (CA)	Avnaim-Katav *et al.* (2017)	122–222	18	Dead, 0–1 cm
Talbot Creek (OR)*	Milker *et al.* (2016)	93–245	16	Dead, 0–1 cm
Tijuana (CA)	Avnaim-Katav *et al.* (2017)	178–246	17	Dead, 0–1 cm
Zeballos (BC)	Patterson *et al.* (1999)	84–217	38	Dead, 0–1 cm

The modern training set used to constrain the weighted averaging and Bayesian transfer functions was compiled from existing studies that tabulated species counts and sample elevations at salt marshes in California (CA), Oregon (OR), Washington (WA), and British Columbia (BC). The number of samples (N) in each dataset reflects removal of samples with counts of fewer than 30 individuals. Sample type lists the assemblage used (live, dead, or total) and the thickness of surface sediment.

*Sites used by Milker *et al.* (2016) and that comprise the Oregon modern training set in this study. All of the above sites are included in the West Coast modern training set in this study. Because of differences in tidal range among sites, the range of sampled elevations is expressed as a standardized water-level index (SWLI), in which a value of 200 equates to local mean higher high water, and 100 is local mean tide level.

were combined into a single group. *Trochamminita irregularis* and *Trochamminita salsa* were combined as *Trochamminita* spp. Counts of testate amoebae, unidentified foraminifera, and juvenile foraminifera that could not be identified to the species or genus level were excluded. Species abundances were expressed as raw counts. In studies where raw counts were not readily available (Niawiakum; Sabean, 2004), we used the methods described by the original author to estimate a total count size from which counts of individual taxa were estimated. We excluded samples with fewer than 30 foraminifera because such low abundances may indicate that the assemblage is not *in situ* and/or may not be representative of the environment from which the sample was collected. The standardized modern training set is provided as Ⓔ Table S1 (available in the electronic supplement to this article).

Species in the modern training set that occur only in a small number of samples and comprise only a small proportion of individuals in those samples are likely to have a poorly constrained (uncertain) relationship to tidal elevation. We used the approach proposed by Telford (see Data and Resources) to identify and subsequently exclude such species. Briefly, a plot relates the number of samples in which a species is very abundant (termed effective occurrences and measured using the Hill's N2 metric; Hill, 1973) to the standard deviation of its optima (i.e., the tidal elevation at which

it is most abundant) estimated through bootstrapping in a WA transfer function. Telford proposed that species with high N2 have a better-constrained (less uncertain) relationship to tidal elevation than those with low N2, as evidenced by their correspondingly small/large standard deviations. A break in slope on the plot indicates the N2 cutoff value that should be used to exclude taxa from the modern training set. For our modern training set, taxa with N2 of less than six were excluded prior to calibrating the transfer functions. These taxa were *Eggerrella advena*, *Psammosphaera* spp, *Paratrochammina haynesi*, *Saccammina atlantica*, *Trochammina* cf. *nana*, and *Trochammina ochracea*. Only 72 total tests of these taxa appeared in the modern training set compared to a total of more than 125,000 individual foraminifera. These taxa were not present in samples representing the A.D. 1700 earthquake or in the transplant study of Engelhart, Horton, Nelson, *et al.* (2013).

Development of Modern Training Sets

The most recent modern training set of foraminifera employed to reconstruct coseismic subsidence along the Cascadia subduction zone using a transfer function was compiled by Milker *et al.* (2016) using previously published and new datasets from Oregon (Table 1). We generated a modern training set (called Oregon) in which we restricted the composition of our standardized training set to the eight

sites used by Milker *et al.* (2016; Table 1). Along the Pacific coast of North America, several additional studies provide empirical data that constrain the relationship between salt-marsh foraminifera and tidal elevation. The West Coast modern training set is composed of 393 samples drawn from 19 sites between southern California and Vancouver Island (Table 1; Figs. 1 and 2). Collectively, these samples span elevations from 46 to 252 SWLI; we consider the latter to be the highest occurrence of foraminifera. This expanded dataset includes studies that sampled slightly different thicknesses of surface sediment (0–1, 0–1.5, and 0–2 cm; Table 1) and different populations of foraminifera (dead or total; Table 1). The dead assemblage is widely considered to be the most appropriate population for reconstructing RSL using agglutinated salt-marsh foraminifera (e.g., Horton, 1999; Culver and Horton, 2005; Milker *et al.*, 2015), although the total (live plus dead) assemblage may also be used (Scott and Leckie, 1990; Jennings *et al.*, 1995). We included the total assemblage tabulated by Jennings and Nelson (1992) because, on average, fewer than one-quarter of total individuals in any given sample were categorized as live, and we therefore decided that the benefit of including this benchmark dataset (samples from transects spanning a long environmental gradient at three sites) outweighed the potential bias introduced through preferential preservation, patchiness (e.g., Kemp *et al.*, 2011), and/or seasonality of some species (e.g., Horton, 1999). The sites used do not represent an exhaustive list of all surveys of surface foraminifera on the Pacific coast of North America, but we limited inclusion to published studies that systematically sampled the elevational gradient, accurately measured elevation, and provided readily available tabulated data.

Simulated Coseismic Subsidence

To simulate coseismic subsidence, Engelhart, Horton, Nelson, *et al.* (2013) performed a field-based experiment at Hidden Creek, South Slough, Oregon (Fig. 1), in which a bed of modern, high salt-marsh sediment was transplanted to an adjacent tidal-flat environment that was 0.64 m lower, where it was rapidly ($\sim$14 mm/yr) buried by mud. The amount and abruptness of elevation change were thought to be similar to a great earthquake along the Cascadia subduction zone. A core collected 5 yrs later through the transplanted block and overlying muddy sediment was analyzed for foraminifera and provides an opportunity to test how accurately the four transfer functions can reconstruct changes in tidal elevation caused by coseismic subsidence. Counts of foraminifera from the transplant plot were standardized following the approach described for modern samples (see the Standardization of Modern Training Sets section).

Biosedimentary Record of the A.D. 1700 Earthquake

Beneath tidal marshes along the Pacific coast of North America, the A.D. 1700 earthquake is represented by a sharp stratigraphic contact that separates pre-earthquake, organic-rich sediment (peat or soil) deposited in a high salt-marsh or upland environment from overlying, postearthquake sediment composed of inorganic mud that accumulated in a low salt-marsh or tidal-flat environment. This sharp stratigraphic change coupled with microfossil assemblages preserved within the two sediment units indicate abrupt RSL rise. We compiled published counts of foraminifera that record the A.D. 1700 earthquake at 13 sites from southern Oregon to Vancouver Island (Fig. 1) and accepted the original authors' interpretation that they represent the A.D. 1700 earthquake. In all but two instances (Nestucca Bay and Netarts Bay, Oregon), these sites also provided data on the modern distribution of foraminifera. The data were standardized following the approach described for modern samples (see the Standardization of Modern Training Sets section).

Methods

Development and Application of Weighted-Averaging Transfer Functions

We generated two WA transfer functions (with classical deshrinking; see e.g., Juggins and Birks, 2012) using the software C2 (Juggins, 2011), in which species abundance was expressed as a percentage calculated from raw counts in each sample. The first WA transfer function (WA Oregon) was calibrated using the Oregon training set ($n = 169$ modern samples; Table 1). The second WA transfer function (WA West Coast) was calibrated using the West Coast training set ($n = 393$ modern samples; Table 1). Neither modern dataset was screened to remove outliers because the original publications did not identify any samples as being ecological outliers at the time of collection, and we therefore consider both datasets to capture natural variability. Transfer-function performance was measured through *n*-fold cross validation ($n = 10$).

When applied to fossil assemblages of foraminifera, the WA Oregon and WA West Coast transfer functions return an estimate of the tidal elevation at which the sample originally accumulated with a sample-specific ($\sim$1σ) uncertainty (e.g., Juggins and Birks, 2012). Reconstructed tidal elevation is in SWLI units and is converted to an absolute elevation using the modern, observable tidal range at the site under investigation. This approach therefore assumes that tidal range was stationary through time.

Development and Application of Bayesian Transfer Functions

Following the approach described in Cahill *et al.* (2016), we developed a BTF using the West Coast modern training set in which species abundances were expressed as raw counts. This approach assumes a multinomial distribution for foraminiferal assemblages, and uses a set of penalized spline smoothing functions (Lang and Brezger, 2004) to describe the nonlinear relationship between each foraminiferal taxa and tidal elevation. The multinomial distribution models raw

counts (rather than percentage) and is used for computing probabilities when there are more than two possible outcomes (e.g., the probability of occurrence for multiple species of foraminifera at a single elevation). The parameters that describe each taxa's response curve were estimated from the modern training set using Markov chain Monte Carlo sampling (e.g., Brooks *et al.*, 2011). Performance of the BTF was measured through *n*-fold cross validation ($n = 10$). When applied to fossil assemblages of foraminifera, the BTF returns a reconstructed tidal elevation (in SWLI units), with a sample-specific 95% uncertainty interval. This uncertainty interval partly reflects count size, in which samples with large counts can reduce uncertainty, and results from samples in which few individuals were counted can be correspondingly uncertain. For comparison with results from the WA transfer functions, we present 1σ results from the BTF throughout the article and in all figures.

The BTF can further and formally constrain reconstructions of tidal elevation through the inclusion of prior information (e.g., Cahill *et al.*, 2016). We applied the BTF to assemblages of foraminifera representing simulated and actual earthquake-induced subsidence in two different ways. In the first instance, no prior information was included, and all fossil samples were assigned an uninformative prior, which assumed that all fossil samples most likely formed at an elevation between 40 and 252 SWLI (a conservative treatment of the range of sample elevations in the West Coast modern training set). In the second instance, we assigned informative priors to fossil assemblages, based on the reported stratigraphic context of the sample. Samples described as clastic-dominated tidal-flat or low salt-marsh sediment were assumed to have accumulated between local mean low water ($\sim$20 SWLI, but site specific) and MHHW (defined as 200 SWLI at all sites). Organic-rich, peaty samples described as having accumulated in a high salt-marsh environment were assigned priors of local MHW ($\sim$180 SWLI, but site specific) to the highest occurrence of foraminifera in the West Coast modern training set (252 SWLI). These priors arose from our own observations of modern sedimentary environments along the Cascadia subduction zone and those reported in other studies (see the Tectonic Setting, Glacio-Isostatic Adjustment, and Tidal-Marsh Zonation section). Informative priors do not set hard limits on the tidal elevations that can be reconstructed; rather they increase the probability that reconstructed tidal elevation falls within the specified prior range. Consequently, our approach is compatible with the possibility that, in rare and localized circumstances, the pattern of sediment distribution can depart from the prevailing, regional-scale pattern that we described previously. Our assumed upper limit (MHHW) for tidal-flat and low salt-marsh sediment is conservative, as is our assumed lower limit (MHW) for high salt-marsh sediment. Overlap in the specified ranges of these groups allows the BTF to reconstruct coseismic subsidence, coseismic uplift, or no change in tidal elevation. In setting priors, we elected to use only descriptions of sediment characteristics and stratigraphic context because this is the most robust field-based evidence of subsidence during

the A.D. 1700 Cascadia earthquake, is grounded in geological reasoning, and allows all cores to be treated in a uniform fashion because quantitative sediment characterizations (e.g., through grain-size analysis or loss-on-ignition measurements) and results from secondary proxies (e.g., counts of diatoms, testate amoebae, or δ^{13}C measurements) are available only for some sites. However, the BTF can accommodate prior information that is diverse and core specific.

Estimating Coastal Subsidence

We estimated coastal subsidence as the difference in reconstructed tidal elevation between a pre-earthquake sample and a postearthquake sample in the same core. The same pairs of pre-earthquake and postearthquake samples were used to estimate coastal subsidence from each of the four transfer functions. To identify these samples, we excluded assemblages from tsunami deposits because they are often dominated by tests transported from subtidal environments by the incoming wave and also by tests from higher environments by the retreating wave, which results in a mixed and allochthonous population (e.g., Hawkes *et al.*, 2007; Mamo *et al.*, 2009; Pilarczyk *et al.*, 2012). We limited our analysis to samples that yielded a minimum of 30 foraminifera (the same threshold set for inclusion in the modern training set) and had a modern analog in the West Coast modern training set. We measured the analogy between modern and fossil samples using the Bray–Curtis distance metric. If the dissimilarity between a fossil sample and its closest modern analog was less than the 20th percentile of dissimilarity measured between all possible pairings of modern samples, then the fossil sample was deemed to have a modern analog (e.g., Jackson and Williams, 2004; Simpson, 2012). The 20th percentile is an appropriate threshold for salt-marsh foraminifera because of the low species diversity exhibited by most assemblages (Kemp and Telford, 2015).

For subsidence calculated using WA transfer functions, we estimated an accompanying uncertainty using the following equation:

$$\text{subsidence uncertainty} = \sqrt{(E_{\text{pre}}^2 + E_{\text{post}}^2)},$$

in which E_{pre} is the $\sim$1σ uncertainty for reconstructed tidal elevation in the pre-earthquake sample, and E_{post} is the $\sim$1σ uncertainty for reconstructed tidal elevation from the postearthquake sample. The BTF generates a large number of posterior tidal elevation reconstructions for the pre-earthquake and postearthquake samples using Markov chain Monte Carlo sampling. From this suite of individual reconstructions samples (numbered 1st…*j*th…*n*th), a posterior probability distribution is created. Subsidence was estimated by calculating the difference between tidal elevation reconstructions from the *j*th posterior pre-earthquake sample and the *j*th posterior postearthquake sample, as shown in the following equation:

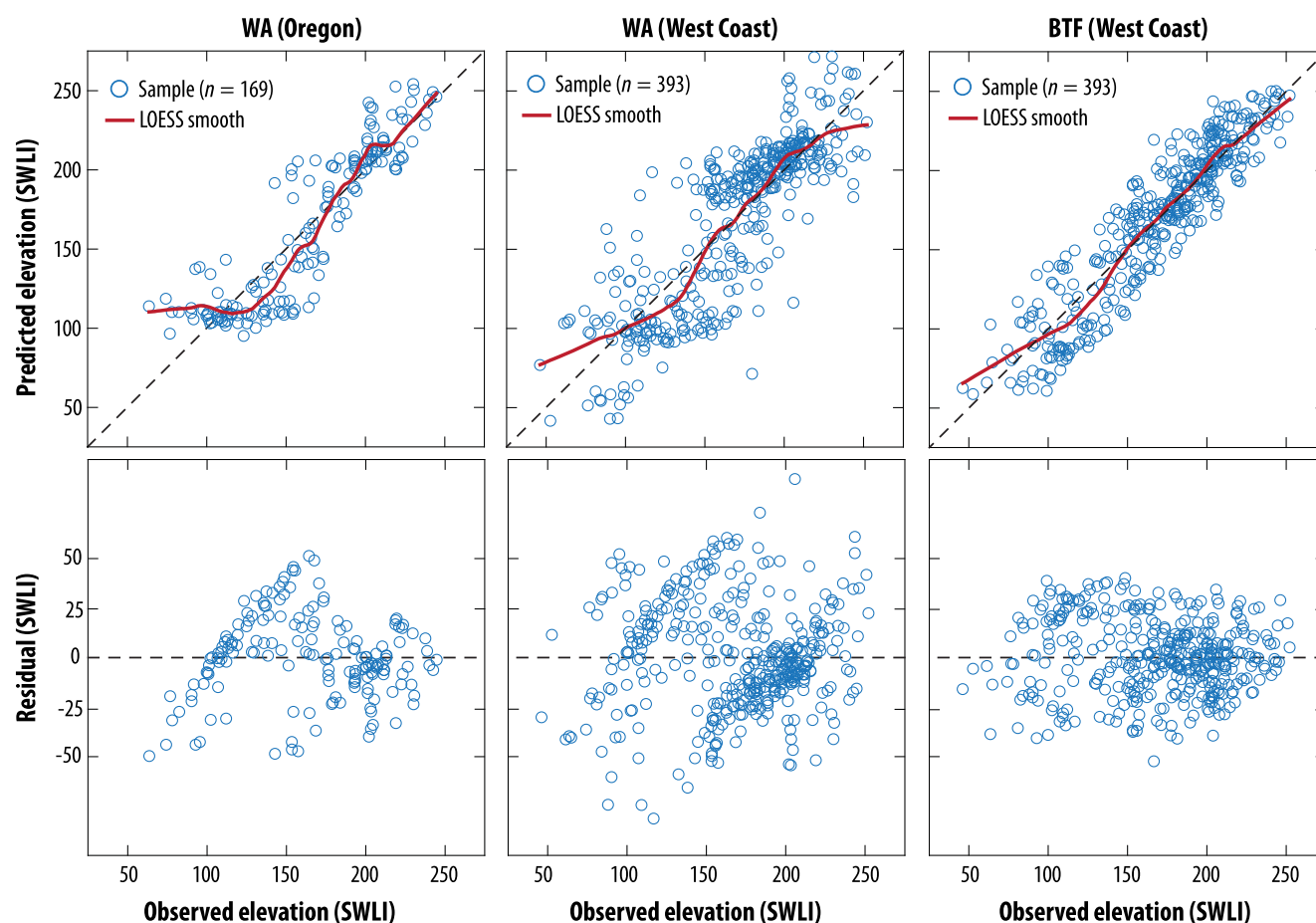$$E_{\text{pre}}(j) - E_{\text{post}}(j).$$

Figure 3. Cross validated transfer-function performance. Columns of panels represent three different transfer functions produced using different datasets and numerical methods. The modern training set for the weighted averaging (WA) Oregon transfer function includes samples only from the eight sites in Oregon used by Milker *et al.* (2016). The West Coast modern dataset used in the WA West Coast transfer function and in the Bayesian transfer function (BTF) includes samples from 19 sites from southern California to Vancouver Island, British Columbia. WA transfer functions used classical deshrinking. For each transfer function, results are from *n*-fold cross validation (*n* = 10). Top row of panels show observed elevation (i.e., measured in the field at the time of sample collection) versus predicted elevation (i.e., reconstructed by the model through cross validation). Solid lines are a best fit estimated using locally weighted smoothing (LOESS). The bottom row of panels show difference between observed and predicted elevation (termed residuals). Dashed one-to-one lines are shown for reference. All sample elevations are expressed as an SWLI, for which a value of 100 corresponds to local MTL, and a value of 200 corresponds to local MHHW. The color version of this figure is available only in the electronic edition.

The mean subsidence estimate and its uncertainty are based on the corresponding distribution for the differences. For direct comparison with the results from WA transfer functions, we use the 1σ range to describe BTF-generated subsidence uncertainties throughout the article.

At some locations, the A.D. 1700 earthquake caused a freshwater, upland environment characterized by soil formation to be subsided into the intertidal zone. In these instances, foraminifera are absent from the pre-earthquake samples, and no tidal elevation reconstruction can be generated. The lowest absence of salt-marsh foraminifera in the West Coast modern training set occurred at 236 SWLI in a sample from Salishan Spit (Fig. 2). We therefore assumed that pre-earthquake soil lacking foraminifera occurred at, or above, 236 SWLI, and subsidence is therefore the difference in elevation between 236 SWLI and the postearthquake

reconstruction of tidal elevation, with an uncertainty that is the same as that for the tidal elevation reconstruction. This approach provides a minimum subsidence estimate.

Results

Transfer Function Performance

Sample elevations in the WA Oregon transfer function span an observed (i.e., measured at the time of sample collection) elevational range of 77–245 SWLI. There is a strong correlation between observed and predicted (estimated by cross validation) elevation (Fig. 3), except at observed elevations below ~150 SWLI. The absolute values of residuals (difference between observed and model-predicted elevation) averaged 16 SWLI, with a standard deviation of 14
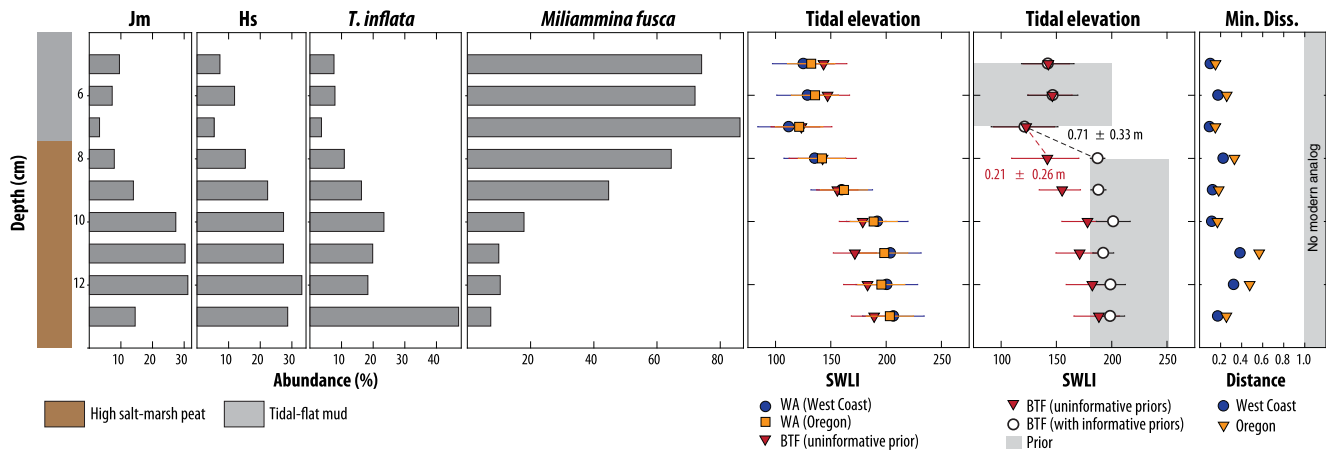
Figure 4. Subsidence reconstructed from the transplant experiment performed by Engelhart, Horton, Nelson, *et al.* (2013). A block of high salt-marsh peat was transplanted into the adjacent tidal-flat environment where ~7 cm of mud accumulated on top of it over the following 5 yrs. The relative abundance of the four most common taxa (96% of counted individuals) of foraminifera are shown (Jm, *Jadammina macrescens*; Hs, *Haplophragmoides* spp; *T. inflata*, *Trochammina inflata*). Tidal elevation (expressed as an SWLI) was reconstructed using WA transfer functions and BTFs. 1σ uncertainties are presented for all transfer functions. The Oregon modern training set was limited to the sites used by Milker *et al.* (2016), whereas the West Coast modern training set was generated from foraminifera counts and elevation measurements from 19 sites. Informative priors used in the BTF (shaded regions) assumed that the high salt-marsh peat formed between local mean high water (MHW) and the highest occurrence of foraminifera in the West Coast modern training set (181–252 SWLI) and that the mud accumulated at an elevation from local mean low water to MHHW (19–200 SWLI). The dissimilarity between each sample in the core and its closest analog in the Oregon and West Coast modern training sets is expressed as a proportion of the threshold used to determine if samples have an appropriate modern analog (the 20th percentile of dissimilarity measured between all possible pairings of modern samples). Therefore, samples with a value of less than 1 are deemed to have a modern analog. Dissimilarity data are presented in this fashion because the absolute thresholds differ between the two datasets. The color version of this figure is available only in the electronic edition.

SWLI and a maximum of 51 SWLI. A noticeable relationship between residuals and observed elevation indicate that the WA Oregon transfer function systematically overpredicts the elevation samples that formed below ~125 SWLI, which could potentially result in postearthquake tidal elevation reconstructions that are too high and consequently coseismic subsidence reconstructions that are too small.

Sample elevations in the WA West Coast transfer function span an observed range of elevation of 46–252 SWLI. This model exhibits a slight tendency to overpredict the elevation of samples from the lowest part of the elevation gradient and underpredict the elevation of samples at the highest observed elevations (Fig. 3). The absolute residuals were 22 SWLI on average with a standard deviation of 17 SWLI and a maximum of 108 SWLI. However, there is no visible structure in the residuals, indicating that systematic bias in predicted elevations is likely weak.

For the BTF calibrated using the West Coast modern training set (Fig. 3), there is a strong correlation between observed and predicted elevations along the full environmental gradient, although a modest tendency to overpredict the elevation of low samples is noted. The absolute residuals in this transfer function averaged 15 SWLI, with a standard deviation of 11 SWLI and a maximum of 53 SWLI. The lack of any relationship between residuals and observed elevation indicates that the BTF produces unbiased reconstructions of elevation.

Replication of Simulated Subsidence

The Engelhart, Horton, Nelson, *et al.* (2013) experiment simulated 0.64 m of coseismic subsidence by transplanting a block of high salt-marsh peat to an adjacent tidal flat where it was buried by mud. The core collected 5 yrs later shows a sharp stratigraphic contact between pre-earthquake and postearthquake sediment. The pre-earthquake high salt-marsh peat unit is dominated by *Jadammina macrescens*, *Trochammina inflata*, and *Haplophragmoides* spp (Fig. 4). However, the uppermost part of this unit also includes high (up to 64%) abundances of *Miliammina fusca*, which Engelhart, Horton, Nelson, *et al.* (2013) interpreted as faunal mixing across the stratigraphic contact. The postearthquake assemblage of foraminifera in the mud unit is dominated by *Miliammina fusca* (72%–86%). All samples in the core had modern analogs in both the Oregon and West Coast modern datasets and yielded counts greater than 30 individuals. We therefore used the samples at 8 and 7 cm as the pre-earthquake and postearthquake samples, respectively. Both WA transfer functions and the BTF with uninformative priors estimated mean subsidence of 0.20–0.25 m, which is considerably less than the known change of 0.64 m. The BTF with informative priors reconstructed subsidence of 0.71 ± 0.33 m.

Subsidence in A.D. 1700

To reconstruct subsidence caused by the A.D. 1700 Cascadia earthquake, we applied the four transfer functions
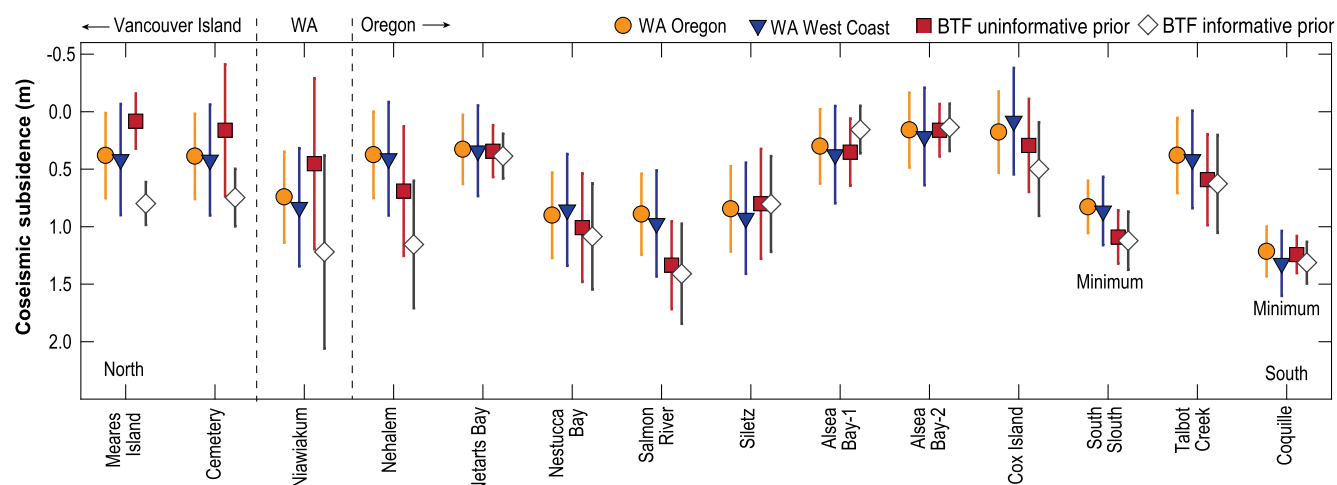
Figure 5. Subsidence caused by the A.D. 1700 Cascadia earthquake at 13 sites along the Pacific coast of North America (note that the two independent reconstructions from Alsea Bay, Oregon, are differentiated). Reconstructions are shown for four different transfer functions represented by distinctive symbol shapes and shading. Uncertainties are 1σ, and sites are organized from north to south. The color version of this figure is available only in the electronic edition.

to foraminifera preserved in 14 cores or sections of coastal sediment from 13 sites in Oregon, Washington, and Vancouver Island (Fig. 5) that include an abrupt stratigraphic contact representing coseismic subsidence. At two of these sites (Coquille and South Slough), our analysis yielded minimum estimates of subsidence because the pre-earthquake sediment was soil that did not support a population of foraminifera by virtue of lying above the reach of tides (Hawkes *et al.*, 2011; Engelhart, Horton, Vane, *et al.*, 2013). There was a strong geographic pattern of subsidence within each transfer function (Fig. 5) that showed relatively large (> 0.5 m) land-level changes in southern Oregon (at Coquille, Talbot Creek, and South Slough) and smaller changes (∼0.25 m) in the region centered on Alsea Bay, Oregon. There was a second region of large subsidence (> 1.0 m) centered on Salmon River, Oregon, and a return to smaller changes (< 0.5 m) at sites in northern Oregon (Netarts Bay). A third region of large land-level changes occurred at Nehalem, Oregon, and at Niawiakum, Washington. On Vancouver Island, the Cemetery and Meares Island sites recorded relatively small (< 1.0 m) amounts of subsidence. Comparison of subsidence reconstructions derived from the four different transfer functions shows overlap of their 1σ uncertainties (Fig. 5). However, mean subsidence estimates do vary among some transfer functions. The most pronounced difference occurred between the WA Oregon transfer function and the BTF with informative priors that were constrained by the West Coast modern training set (Fig. 6, first row). In this comparison, the BTF yielded a greater mean subsidence estimate at 10 of the 13 sites, and the difference at these 10 sites ranged from 0.06 to 0.78 m, which is 8%–221% larger than the WA Oregon reconstruction. The variability of subsidence estimates among transfer functions has a spatial pattern, with the greatest differences from Vancouver Island to northern Oregon (Nehalem) and smaller differences south of Netarts Bay, Oregon (Fig. 5).

Geographic Distribution of Foraminiferal Assemblages

We sought to objectively identify assemblages of foraminifera and to establish where (vertically and geographically) these assemblages are present on modern tidal marshes along the Cascadia subduction zone. This analysis is important for reconstructing coseismic subsidence because it provides insight into which assemblages are likely (and unlikely) to be encountered in the stratigraphic record in particular regions. We applied partitioning around medoids (PAM; Rousseeuw, 1987; Kaufman and Rousseeuw, 2005) to the West Coast modern training set to identify assemblages. PAM seeks to minimize within-assemblage variance while maximizing variance among assemblages. We determined the number of assemblages (5; Table 2) by calculating the maximum-average-silhouette width for 2–20 groups. Silhouette widths are a measure of how well a sample fits into the assemblage that it is assigned to (i.e., how similar it is in faunal composition to other samples in the same assemblage), where widths close to 1 (maximum possible value) indicate that a sample was classified appropriately, whereas values close to −1 (minimum possible value) reflect poor classification. Nonmetric multidimensional scaling (e.g., Kruskal, 1964; Kenkel and Orlóci, 1986) was used to conveniently visualize the relationship among the five assemblages of modern tidal-marsh foraminifera and their relationships to tidal elevation (Fig. 7).

High salt-marsh environments are represented by assemblages 1–4. Assemblages 1 (*Jadammina macrescens*) and 2 (*Haplophragmoides* spp and *Trochammina inflata*) are present from British Columbia to southern California. Assemblages 3 (*Trochamminita* spp) and 4 (*Balticammina pseudomacrescens*; Fig. 7) were not recorded in southern California (Avnaim-Katav *et al.*, 2017). These assemblages occupy the very highest parts of the intertidal zone (Fig. 2) and could be missed
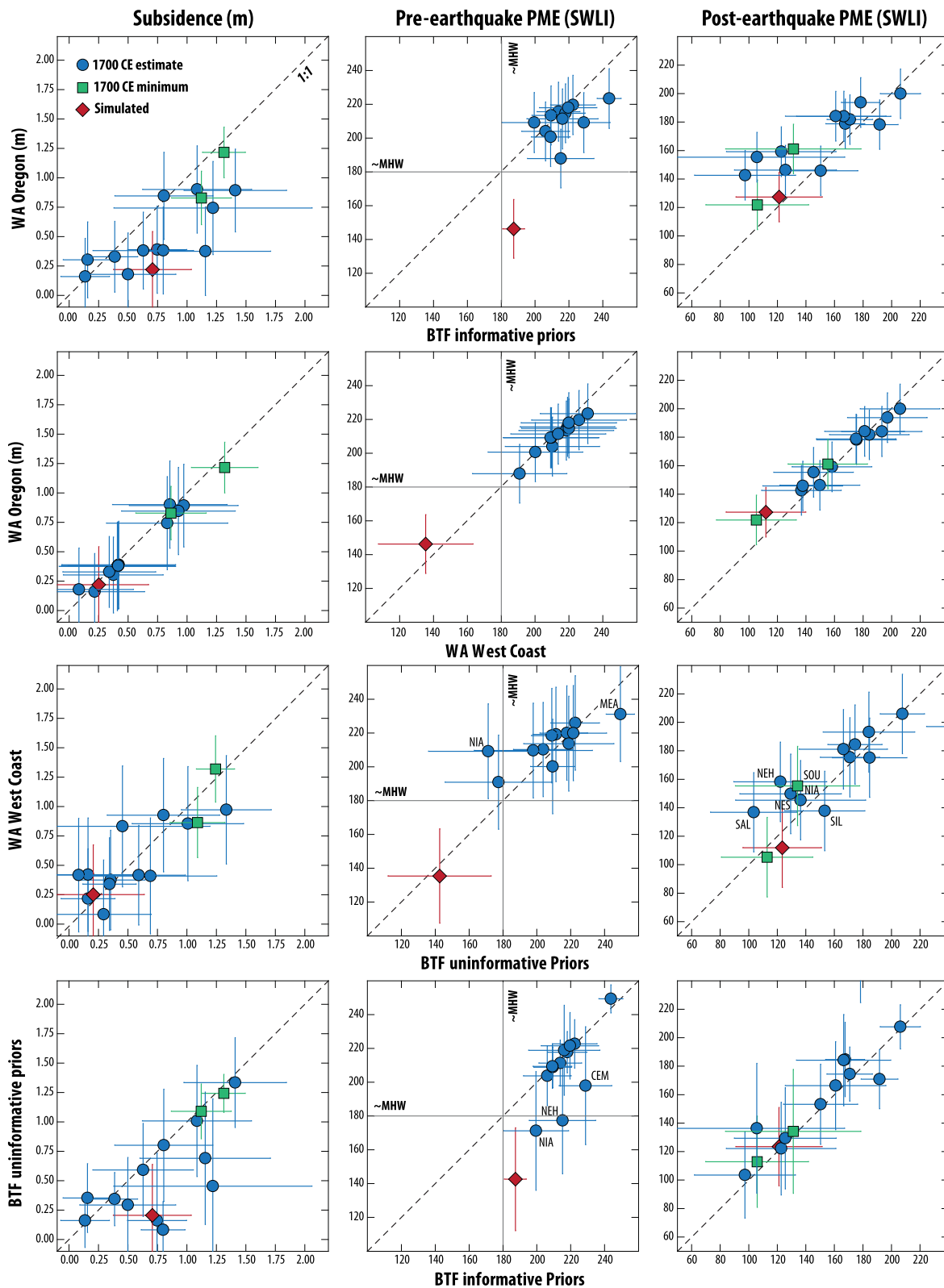
Figure 6.   Pairwise comparisons of model reconstructions (rows) for subsidence (left column), paleomarsh elevation (PME) estimated for the pre-earthquake sample (center column; the approximate elevation of local MHW is shown for reference), and PME estimate for the postearthquake sample (right column). Error bars represent 1σ uncertainties. PME is expressed as SWLI in which a value of 100 is MTL and 200 is MHHW. Symbol shape and shading identifies reconstructions from the A.D. 1700 earthquake and the field-based simulation. Dashed lines represent parity between models and are shown for reference. MEA, Meares Island; NES, Nestucca; SOU, South Slough; SAL, Salmon River; NIA, Niawiakum; NEH, Nehalem; SIL, Siletz. The color version of this figure is available only in the electronic edition.
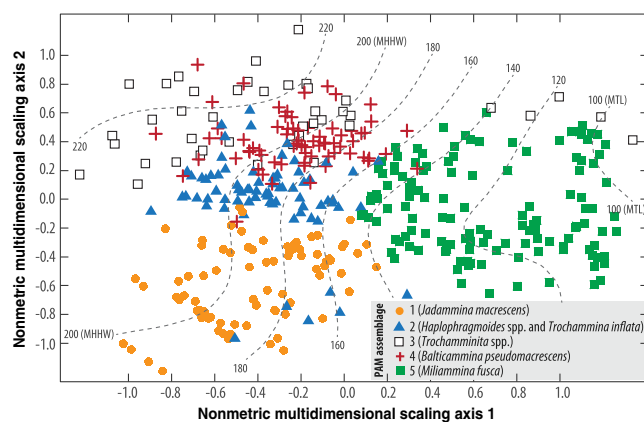
Figure 7. Ordination of the West Coast modern training set using nonmetric multidimensional scaling. Symbol shape and shading represents the assemblage that each sample was assigned to using partitioning around medoids (PAM); the characteristic species of each assemblage are listed in the legend. Dashed lines mark elevation contours where elevation is expressed as an SWLI in which a value of 100 corresponds to MTL and a value of 200 is defined as MHHW. The color version of this figure is available only in the electronic edition.

by studies in which the sampling regime does not extend across the salt marsh to upland transition. However, samples from Seal Beach and Tijuana were concentrated in the high salt-marsh environments where these assemblages were found elsewhere, and it is therefore unlikely that their absence can be attributed to a sampling regime that simply missed the assemblage. The absence of assemblages 3 and 4 in Washington likely reflects local-scale variability, because there is only a single site from the state in our expanded modern training set. The widespread nature of assemblages 1 and 2 and the geographically restricted nature of assemblages 3 and 4 is likely to be mirrored in the recent stratigraphic record where these high salt-marsh assemblages are characteristic of pre-earthquake sediment. Therefore, the geographic scope of the training set will influence coseismic subsidence reconstructions by providing (or failing to provide) modern analogs. For example, efforts to reconstruct coseismic subsidence caused by one earthquake at many sites along the

Pacific coast would need to utilize a geographically diverse training set that includes sites where assemblages 3 and 4 are present today. In contrast, efforts to reconstruct multiple coseismic subsidence events at a single site could reasonably use a training set of limited geographic scope because some assemblages are unlikely to be encountered in the stratigraphic record.

Tidal-flat and low salt-marsh environments are characterized by assemblage 5, in which *Miliammina fusca* is the dominant species. Although *Miliammina fusca* was present, this assemblage was not recorded by Avnaim-Katav *et al.* (2017) in southern California, likely because the sampling regime at these locations did not extend to sufficiently low elevations to capture it (only one sample across the two sites was recovered from below local MHW; Fig. 2a). Other studies from California (including southern California) reported tidal-flat and low salt-marsh assemblages with high abundances of *Miliammina fusca* (e.g., Scott *et al.*, 1996). A *Miliammina fusca*-dominated zone is therefore likely to be a feature of salt marshes along the entire Pacific coast of North America, because it is along the Atlantic coast (e.g., Wright *et al.*, 2011).

Differences in Coseismic Subsidence Reconstructions among Transfer Functions

The most pronounced difference in reconstructed coseismic subsidence among transfer functions is the systematic difference between the WA Oregon transfer function and the BTF with informative priors that was calibrated using the West Coast modern training set (Fig. 6, first row). We use three pairwise comparisons of transfer functions to explore why this difference occurs and to examine its implications for reconstructing earthquake-induced RSL change along the Cascadia subduction zone using foraminifera and transfer functions. These comparisons focus on how tidal elevation reconstructed from pre-earthquake and postearthquake sediment samples subsequently influences estimates of subsidence. Specifically, we investigate the influence of (1) modern training-set composition, (2) taxa–elevation relationships that are not unimodal, and (3) postdepositional faunal mixing.

Modern Training-Set Composition

Reconstructions of tidal elevation from transfer functions necessarily reflect the characteristics of the modern training set used to calibrate them. A pairwise comparison of paleomarsh elevation (PME) reconstructions from the WA Oregon and WA West Coast transfer functions (Fig. 6, second row) allows us to test the contribution to subsidence estimates that arises from expanding the number of samples and geographic range of the modern training set. Both WA transfer functions produce near-identical reconstructions of pre-earthquake tidal elevation from high salt-marsh

Table 2
Assemblages of Tidal-Marsh Foraminifera Identified in the West Coast Modern Training Set

Assemblage	Key Taxa	Elevation (SWLI)	Presence	n
1	*Jadammina macrescens*	182 ± 27	CA, OR, VI	79
2	*Haplophragmoides* spp	190 ± 24	CA, OR, WA, VI	73
	Trochammina inflata			
3	*Trochamminita* spp	208 ± 45	OR, VI	42
4	*Balticammina pseudomacrescens*	189 ± 28	OR, WA, VI	70
5	*Miliammina fusca*	125 ± 31	CA, OR, WA, VI	129

The five assemblages were identified by partitioning around medoids of the West Coast modern training set. Elevation is the mean and standard deviation of samples in the group and is expressed as an SWLI. The number of samples in each group is *n*. The distribution of each assemblage is summarized by its presence in samples collected from California (CA), Oregon (OR), Washington (WA), and Vancouver Island (VI).
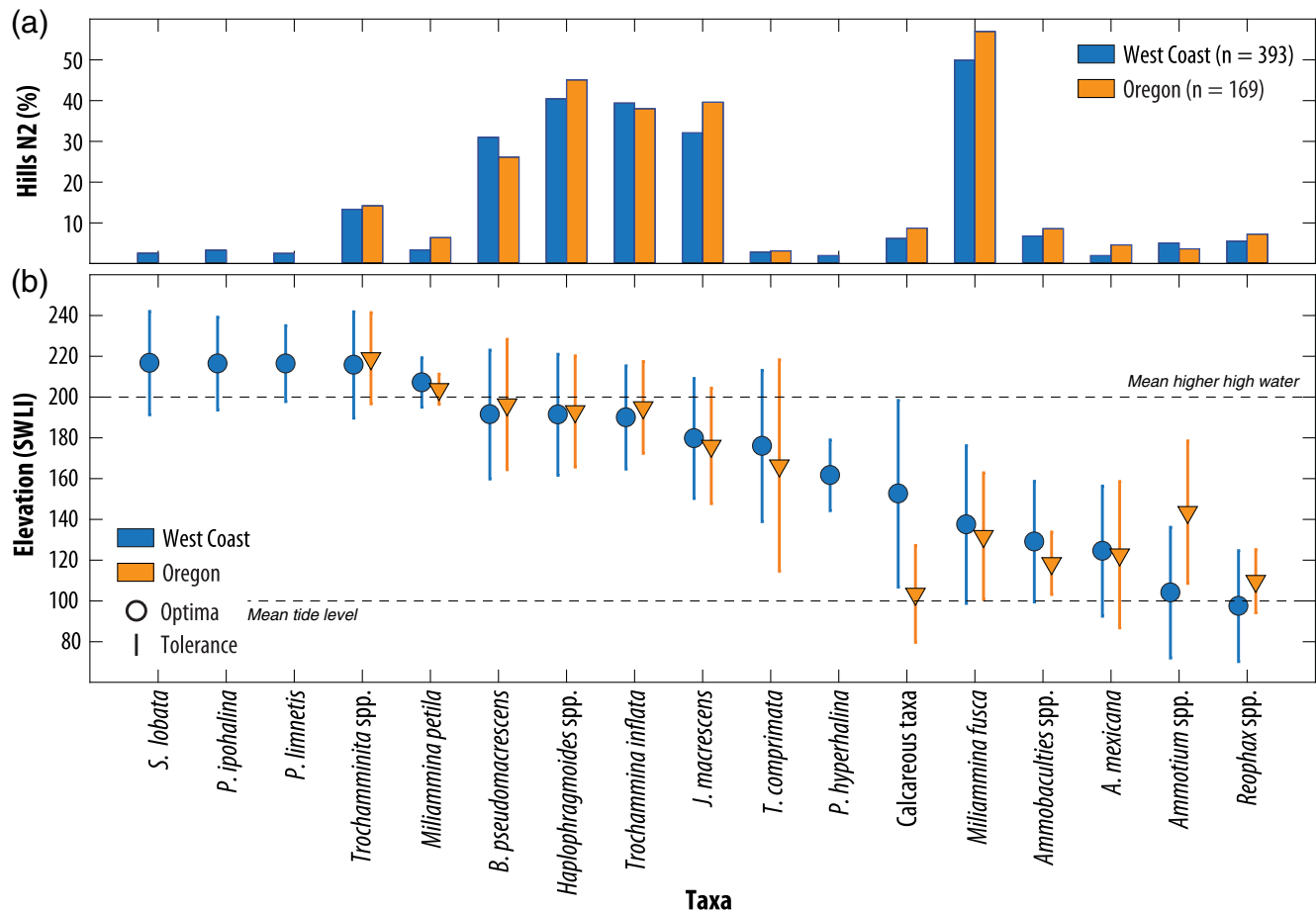
Figure 8. Taxa–elevation relationships predicted using WA transfer functions trained on the Oregon and West Coast training sets (differentiated by shading and symbols). (a) Number of samples (expressed as a percentage of total samples in the training set to aid comparability) in which taxa were very abundant (termed effective occurrences and measured using the Hill's N2 metric; Hill, 1973). (b) Optima (symbols) and tolerance (error bars) of taxa predicted by the two transfer functions. Elevation is expressed as an SWLI. The color version of this figure is available only in the electronic edition.

sediment and assemblages of foraminifera. Similarly, reconstructions of postearthquake tidal elevations are consistent between both WA transfer functions, except for modest differences at Coquille and in the transplant study. The consistency of these reconstructions indicates that taxa–elevation relationships were largely unchanged by expansion of the modern training set, which is further demonstrated by the similarity between the two WA transfer functions of most taxa's optima and tolerance (Fig. 8). Only a small number of taxa have optima and tolerances that differ markedly between the WA transfer functions (e.g., *Reophax* spp, *Ammotium salsum*, and calcareous taxa), and they are rare in both training sets (as evidenced by low Hill's N2 values; Fig. 8). For all but two taxa (*Tiphotrocha comprimata* and *Balticammina pseudomacrescens*), expansion of the modern training set caused tolerances to increase; for the six most common taxa (Fig. 2) the average (absolute) change in tolerance was 5 SWLI. The consistency between training sets of optima and tolerance for the six taxa that together comprise 94% of individuals in the modern training set indicates that taxa–elevation relationships do not vary spatially, which is an assumption that underpins

the use of transfer functions to reconstruct tidal elevation (Juggins, 2013). We conclude that coseismic subsidence reconstructions using WA transfer functions are insensitive to further expansion of regional-scale modern training sets, except if rare taxa are present in relatively high numbers.

Expansion of the modern training set increases the number and variety of analogs available for interpreting fossil assemblages (Horton and Edwards, 2005). Commonly, samples that lack a suitable modern analog are excluded from analysis out of concern that the resulting reconstruction may not be ecologically reasonable (e.g., Simpson, 2012). For example, in their analysis of the Meares Island core using a local-scale modern training set, Wang *et al.* (2013) could only estimate a minimum subsidence (0.49 m) because the postearthquake assemblages lacked a modern analog. In the West Coast modern training set, these samples had modern analogs, and we reconstructed a mean subsidence of 0.08–0.8 m, depending on the model used (Fig. 5). The reduced frequency of no modern analog outcomes when using the West Coast training set enables reconstructions to be generated from more locations than application of the Oregon training set.
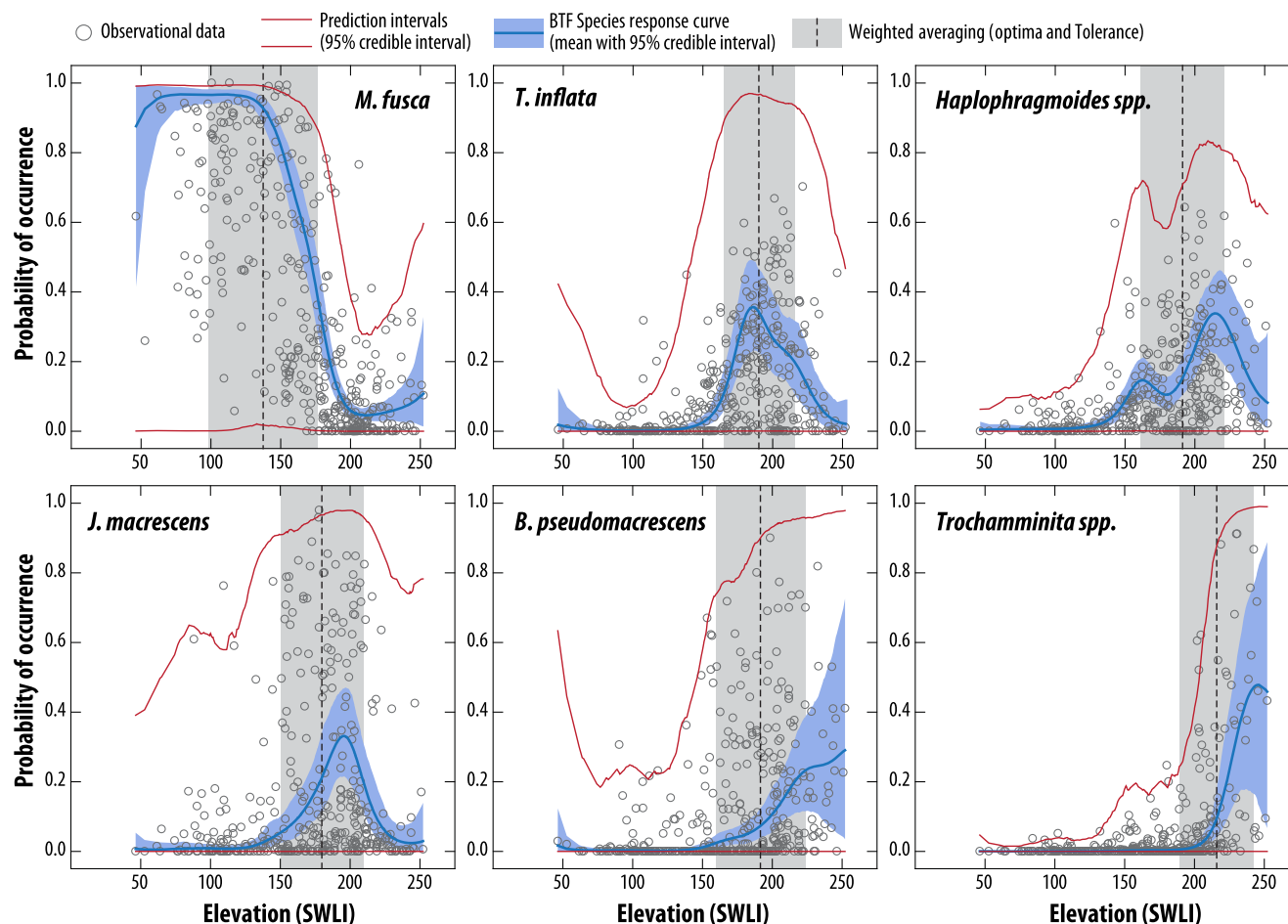
Figure 9. Taxa–elevation relationships predicted by the BTF using the West Coast modern training set. Results for the six most common taxa are shown. For comparison, the optima and tolerance predicted by WA for the same taxa from the West Coast modern training set are presented. The color version of this figure is available only in the electronic edition.

Taxa–Elevation Relationships

Pairwise comparison of the WA West Coast transfer function and the BTF with uninformative priors provides insight into how the assumed form of taxa–elevation relationships influences subsidence reconstructions. WA imposes a unimodal form on all taxa–elevation relationships, which is often ecologically plausible, particularly where long and continuous environmental gradients are sampled in the modern training set (Juggins and Birks, 2012). In contrast, the BTF does not impose a single form of taxa–elevation relationship but instead adopts a more flexible approach in which the form of the relationship is data driven (i.e., determined from the modern training set; Cahill *et al.*, 2016).

The BTF produced response curves for *Trochammina inflata*, *Haplophragmoides* spp, and *Jadammina macrescens* that have an approximately unimodal form (Fig. 9). The optima calculated for these taxa in the WA West Coast transfer function occur close to the elevation at which they are most likely to occur according to the BTF. Therefore, the WA West Coast transfer function and the BTF are unlikely to reconstruct different tidal elevations when applied to assemblages in

which these taxa are dominant (typically pre-earthquake samples from high salt-marsh environments that are present along the entire length of the Cascadia subduction zone; Figs. 2 and 7). This is demonstrated by the consistency at most sites between pre-earthquake tidal elevation reconstructions generated by the WA West Coast transfer function and by the BTF with uninformative priors (Fig. 6, third row).

For *Balticammina pseudomacrescens* and *Trochamminita* spp, a unimodal response curve may not adequately describe the taxa–elevation relationship because the BTF shows that their probability of occurrence increases with elevation until the highest occurrence of foraminifera, above which foraminifera are absent and where the probability of occurrence decreases sharply to zero. This pattern occurs because the transition from the uppermost edge of a salt marsh into the surrounding upland is a sharp ecological boundary for foraminifera because they cannot survive in environments that are above marine influence (e.g., Scott and Medioli, 1978; Edwards and Wright, 2015). This type of relationship may not be adequately described by a unimodal response curve, and consequently the optima of these taxa could be too low in the WA West Coast transfer function. The maximum probability

of occurrence in the BTF for these taxa is higher than the WA-estimated optima (252 SWLI compared to 191 SWLI for *Balticammina pseudomacrescens* and 245 SWLI compared to 216 SWLI for *Trochamminita* spp; Figs. 8 and 9). In fossil samples where either of these two taxa is dominant, the BTF may return a higher reconstruction of tidal elevation than the WA West Coast transfer function. Given the modern vertical and geographic distribution of these taxa (see the Geographic Distribution of Foraminiferal Assemblages section) it is likely that assemblages of foraminifera with high proportions of *Balticammina pseudomacrescens* and *Trochamminita* spp are most likely to be encountered in pre-earthquake sediment and at salt marshes in the northern portion of the Cascadia subduction zone. Intriguingly, the largest discrepancies between coseismic subsidence reconstructions generated using different transfer functions occur north of Netarts Bay (Fig. 5), where these two taxa with nonunimodal relationships to elevation are most commonly encountered. However, the WA West Coast transfer function and the BTF did not generate reconstructions of pre-earthquake tidal elevation that were notably different from one another (Fig. 6, third row). This occurs because the range of elevations tolerated by *Balticammina pseudomacrescens* and *Trochamminita* spp in the WA West Coast transfer function span the same elevations where the BTF predicts that the taxa is most likely to occur (Fig. 9). Therefore, although the form of the taxa–elevation relationships differs markedly between the two types of transfer function, this had little practical effect on reconstructed tidal elevation. We note that assemblages of diatoms used to reconstruct coseismic subsidence are likely less prone than foraminifera to this ecological edge effect at the upper edge of salt marshes because they exist across adjacent freshwater, brackish, and marine environments. (e.g., Dura, Hemphill-Haley, *et al.*, 2016; Sawai *et al.*, 2016; Shennan *et al.*, 2016).

From the available data, the BTF assumes a nonunimodal response curve to quantify the relationship between *Miliammina fusca* and tidal elevation (Fig. 9), in which there is a high and consistent probability of occurrence below ~150 SWLI. An assumed unimodal relationship between *Miliammina fusca* and tidal elevation may overestimate the elevation of its optima (resulting in a reconstruction of tidal elevation that is too high) and underestimate its tolerance using the West Coast training set. At sites where the postearthquake sample likely formed between ~100 and ~150 SWLI (Nehalem, Niawiakum, South Slough, Nestucca, Siletz, and Salmon River), the WA West Coast transfer function reconstructs a systematically higher tidal elevation than the BTF with uninformative priors (Fig. 6, third row). At these sites, the postearthquake sample is composed of a mixed assemblage of *Miliammina fusca* (~30%–70%) and high salt-marsh foraminifera. The WA West Coast transfer function generates an intermediate reconstruction of tidal elevation from such a mixed assemblage. In contrast, when *Miliammina fusca* makes up more than ~30% of the assemblage, the BTF with uninformative priors reconstructs a distinct drop in tidal elevation reconstructed from ~180 SWLI (the approximate elevation of

local MHW at most sites) to ~100–140 SWLI. This abrupt change reflects the modern training set, in which the abundance of *Miliammina fusca* declines sharply above ~180 SWLI (Fig. 2b), and also in the species–elevation response curve generated by the BTF, in which the probability of finding *Miliammina fusca* increases sharply below ~180 SWLI (Fig. 9). In samples where *Miliammina fusca* comprises less than ~20%, or more than ~80%, there is little difference between tidal elevation reconstructions from the WA West transfer function and the BTF with uninformative priors.

The form of *Miliammina fusca*'s response curve in the BTF likely reflects a scarcity of available data to constrain the lower elevation at which this species occurs because of the practical difficulties associated with safely sampling tidal flats at low tide. Consequently, there are only six samples from below 75 SWLI in the West Coast modern training set and only 32 samples from below MTL (100 SWLI; Fig. 2). The training set is, therefore, unlikely to capture the lowest elevations at which this species occurs. Descriptions of foraminiferal assemblages from shallow subtidal settings in (for example) Oregon's estuaries and lagoons settings indicate that *Miliammina fusca* is replaced by assemblages dominated by calcareous taxa (Hunger, 1966; Manske, 1968; Murray, 2006). Therefore, we anticipate that the distribution of *Miliammina fusca* along a gradient of elevation could likely be described appropriately using a unimodal relationship if more data were available to constrain the lower limit of this species. Providing these constraints will require additional and systematic sampling below MTL and may resolve differences in tidal elevation reconstructed by the WA transfer functions and BTF.

Postdepositional Faunal Mixing

High salt-marsh peat is typically porous, which facilitates downward mixing of tidal-flat or low salt-marsh sediment and foraminifera following earthquake-induced subsidence. For example, Briggs *et al.* (2014) and Milker *et al.* (2016) used computed tomography to show that mud and silt penetrated into pore spaces in underlying peat units following coseismic subsidence. This postdepositional mixing contaminates pre-earthquake assemblages of foraminifera that were originally dominated by high salt-marsh taxa (e.g., *Balticammina pseudomacrescens*) with tests from postearthquake assemblages (e.g., *Miliammina fusca*). If such mixing occurred, transfer functions will reconstruct a pre-earthquake tidal elevation that is too low, and coseismic subsidence will be correspondingly underestimated. Engelhart, Horton, Nelson, *et al.* (2013) concluded that underprediction of subsidence simulated in the transplant experiment was caused by postdepositional, downward mixing that enriched foraminiferal assemblages beneath the stratigraphic contact with *Miliammina fusca*. By adjusting counts of *Miliammina fusca*, they unmixed the assemblage and showed that a WA transfer function could accurately reconstruct subsidence. However, it is not possible to unmix pre-earthquake assemblages for prehistoric earthquakes (including A.D. 1700) because their original composition is unknown.

Pairwise comparison of tidal elevation and subsidence reconstructions from the BTFs with uninformative and informative priors allows us to investigate whether the formal inclusion of stratigraphic information could compensate for postdepositional, downward mixing of foraminiferal tests (Fig. 6, fourth row). Use of informative priors caused the pre-earthquake tidal elevation in the transplant study to increase from 143 SWLI to 187 SWLI (Fig. 4). By reconstructing a higher pre-earthquake tidal elevation, the BTF with informative priors was the only one of the four transfer functions to reconstruct accurately the measured subsidence (without adjusting the foraminiferal assemblage). Similarly, at Nehalem, Niawiakum, and Cemetery, the addition of informative priors resulted in higher reconstructions of pre-earthquake tidal elevation and therefore more subsidence than the BTF with uninformative priors. We note that this difference was greater in the transplant study than in any of the A.D. 1700 cores, which may indicate that artificial and localized lowering of a small sediment block results in more downward mixing than regional-scale subsidence caused by a great earthquake (Fig. 6). Downward mixing from muds into underlying peat does not appear to impact all sites. In particular, the presence of tsunami-deposited sand acts to insulate the foraminiferal assemblage in the pre-earthquake sediment from contamination by postearthquake sediment and taxa. Despite the possibility of postearthquake colonization by pioneer species and rapid deposition of disturbed sediment that contains mixed taxa (Milker *et al.*, 2016), adopting informative priors did not meaningfully change postearthquake tidal elevation reconstructions (Fig. 6, fourth row).

Implications for Understanding the A.D. 1700 Cascadia Earthquake

Wang *et al.* (2013) used reconstructions of coseismic subsidence from microfossils to test and refine deformation models that estimated the geographic pattern and amount of slip that occurred during the A.D. 1700 earthquake. Comparisons of subsidence predicted by deformation models and reconstructed from coastal sediment indicated that the earthquake was characterized by heterogeneous slip with multiple patches of high-moment release separated by boundaries of low-moment release at Cape Mendocino, Cape Blanco, Alsea Bay, and Netarts Bay (Fig. 10). Subsidence reconstructed using the BTF with informative priors indicates that Wang *et al.* (2013) underestimated subsidence at sites between Alsea Bay and Netarts Bay and also to the north of Netarts Bay (at Nehalem and Niawiakum in particular; Fig. 10), which has several implications for our understanding of the A.D. 1700 earthquake.

Reconstructions from the BTF with informative priors indicate that the amount of coseismic subsidence at Alsea Bay (and by inference the slip in that area during the A.D. 1700 earthquake) was small (Fig. 10). From time to time, the megathrust near Alsea Bay generates small, interplate earthquakes, which is in contrast to slip behavior along most of the Cascadia megathrust where such activity is absent (Tréhu
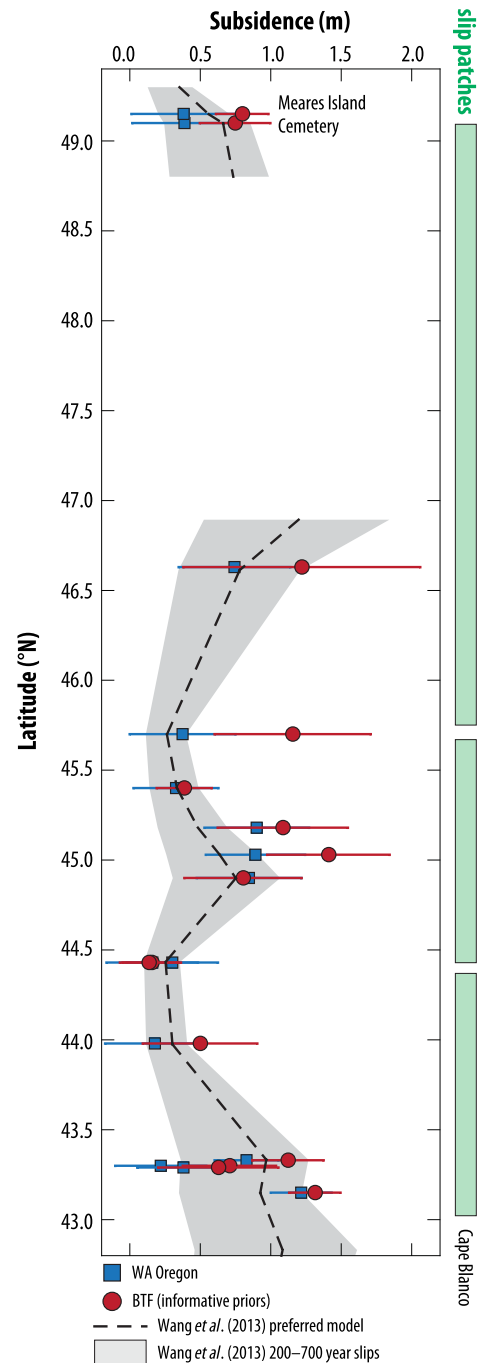

Figure 10. Coastal subsidence reconstructed along the margins of the Cascadia subduction zone using the WA transfer function trained on the Oregon modern dataset (WA Oregon; squares) and the BTF with informative priors that was constrained using the West Coast modern training set (circles). Error bars represent 1σ uncertainties. Results from Coquille and South Slough are estimates of minimum subsidence. The shaded envelope represents the range of subsidence estimated by Wang *et al.* (2013) using models in which heterogeneous rupture occurs with 200–700-yr slips. The dashed line is the preferred model of Wang *et al.* (2013) that was selected because of its ability to reproduce proxy reconstructions of coseismic subsidence. The geographic distributions of slip patches preferred by Wang *et al.* (2013) are represented by shaded bars on the right edge of the figure. The color version of this figure is available only in the electronic edition.

et al., 2015; Wang and Tréhu, 2016). This area also marks an along-strike change in (1) the thickness and distinctness of suddenly submerged tidal deposits in wetland stratigraphic sequences (Nelson and Personius, 1996), (2) the pattern of episodic tremor and slip (Brudzinski and Allen, 2007), (3) a boundary for some of the past megathrust ruptures inferred from offshore turbidite records (Goldfinger *et al.*, 2017), and (4) a boundary for offshore basins inferred from gravity measurements (Wells *et al.*, 2003). Low coseismic slip in this area is consistent with the presence of seamount subduction (Tréhu *et al.*, 2012) that causes megathrust creep accompanied by small earthquakes (Wang and Bilek, 2011).

The relatively small amount of subsidence (∼0.5 m) reconstructed at Netarts Bay supports the inference of Wang *et al.* (2013) that this was also a low-slip area during the A.D. 1700 rupture. However, reconstructions of ∼0.5–1.0 m more coseismic subsidence at sites ∼40 km to the north and south of Netarts Bay (Fig. 10) are challenging to explain and may require sharp along-strike changes in slip amount or rupture geometry. Scaling up of the Wang *et al.* (2013) model to match these subsidence estimates would require coseismic slip exceeding what is equivalent to 700 yrs of subduction (Fig. 10). Wang *et al.* (2013) showed that subsidence off the Oregon coast could be doubled if the down-dip limit of coseismic slip patches were moved farther down-dip (landward) by 30% of their down-dip width. Therefore, the BTF-derived subsidence estimates from ∼46° to ∼47° N (Fig. 10) may require some combination of a wider down-dip width and more abrupt along-strike variations of slip distribution than proposed by Wang *et al.* (2013). Alternatively, the variability in subsidence reconstructions among closely spaced sites could be the result of localized land-level changes (subsidence or uplift) that occurred shortly (hours to years) after the earthquake (Feng *et al.*, 2015) but before assemblages of foraminifera and sediment responded (Horton *et al.*, 2017). Afterslip land-level change could cause coseismic subsidence reconstructions to be too low in the case of additional uplift, or too high in the case of additional subsidence. If there was a large amount of afterslip down-dip of the rupture zone following the A.D. 1700 earthquake, then a wider rupture zone may not be needed. Afterslip may also account for the abrupt along-strike changes in subsidence around Netarts Bay.

Conclusions

Coseismic subsidence caused by great earthquakes along the Cascadia subduction causes abrupt RSL change that can be quantitatively reconstructed from coastal stratigraphy using salt-marsh foraminifera and a transfer function. The geographic pattern of subsidence caused by a single event provides insight into the magnitude and nature of a specific earthquake. We re-estimated subsidence caused by the A.D. 1700 earthquake at sites in Oregon, Washington, and British Columbia using two modern training sets of foraminifera (termed Oregon and West Coast) and two types of transfer function (WA and BTF). The BTF with inform-

ative priors trained on the West Coast modern dataset systematically reconstructed greater subsidence than the WA transfer function trained on the Oregon modern dataset. We examined three possible reasons for this difference.

1. Expansion of the modern training set from 169 samples collected at eight sites in Oregon to 393 samples representing 19 sites from southern California to Vancouver Island did not meaningfully alter taxa–elevation relationships, except for a small number of rare taxa. Therefore, the primary advantage of employing a larger modern training set is the availability of a more diverse suite of analogs for interpreting fossil assemblages of foraminifera. Geographic variability in the modern distribution of high salt-marsh foraminiferal assemblages indicates that pre-earthquake assemblages preserved in recent coastal sediment are also likely to vary among regions. Therefore, reconstructing coseismic subsidence caused by a single earthquake along the Cascadia subduction zone likely requires a correspondingly diverse training set.

2. The BTF indicates that *Balticammina pseudomacrescens* and *Trochamminita* spp do not have a unimodal relationship to tidal elevation because of the sharp ecological boundary between highest salt-marsh environments and surrounding freshwater uplands. Despite an assumption that this relationship is unimodal in the WA transfer functions, there is little practical difference between tidal elevation reconstructions from the two types of transfer function when applied to pre-earthquake samples in which these taxa are abundant. Where postearthquake assemblages include ∼30%–70% *Miliammina fusca*, the BTF reconstructs a lower tidal elevation (greater subsidence) than the WA West Coast transfer function. This occurs because a unimodal response curve does not (yet) adequately describe this species' relationship to elevation, due to the scarcity of samples below ∼75 SWLI in the modern training set.

3. At some sites (particularly those without tsunami sand capping the pre-earthquake sediment), postdepositional, downward mixing of postearthquake sediment, and foraminiferal tests across the sharp stratigraphic contact contaminate pre-earthquake sediments, which results in subsidence reconstructions that are too small. The use of informative priors helped alleviate this problem, as evidenced by the accuracy of the BTF when applied to a field-based experiment that simulated an earthquake.

Our revised subsidence estimates indicate that the A.D. 1700 Cascadia earthquake was characterized by heterogeneous rupture but that slip estimates in patches north of Alsea Bay, Oregon, should be revised upward, although the location of principal slip patches is largely insensitive to model choice. Application of BTFs to microfossil assemblages preserved in coastal sediment provides probabilistic reconstructions of coseismic subsidence that can formally incorporate results from secondary proxies. Further development of BTFs to utilize other types of microfossils (e.g., diatoms)

and secondary proxies (e.g., $\delta^{13}C$) will help further refine the history of megathrust earthquakes along the Cascadia subduction zone and quantify the risk that future events pose to coastal infrastructure and populations.

Data and Resources

The code for identifying species of foraminifera with poorly constrained optima in the modern training set was accessed on Richard Telford's blog (https://quantpalaeo.wordpress.com/2014/05/05/n2-and-the-variability-of-optima/, last accessed September 2017). Counts of modern and fossil foraminifera were downloaded from the original publications, although division of the dead and live assemblages at Cemetery and Meares Island was provided by the original author (Guilbault). The standardized modern training set is provided as an Ⓔ electronic supplement to this article. Tide measurements at Tofino were downloaded from Fisheries and Oceans Canada (http://www.meds-sdmm.dfo-mpo.gc.ca/isdm-gdsi/twl-mne/inventory-inventaire/interval-intervalle-eng.asp?user=isdm-gdsi&region=PAC&tst=1&no=8615, last accessed September 2017). Tidal datums for Zeballos, British Columbia, were obtained through correspondence with the Canadian Hydrographic Service.

References

Atwater, B. F. (1987). Evidence for great Holocene earthquakes along the outer coast of Washington state, *Science* **236,** 942–944.

Atwater, B. F. (1992). Geologic evidence for earthquakes during the past 2000 years along the Copalis River, southern Coastal Washington, *J. Geophys. Res.* **97,** 1901–1919.

Atwater, B. F., and E. Hemphill-Haley (1997). Recurrence intervals for great earthquakes of the past 3500 years at northeastern Willapa Bay, Washington, *U.S. Geol. Surv. Profess. Pap. 1576,* 108 pp.

Atwater, B. F., S. Musumi-Rokkaki, K. Satake, Y. Tsuji, K. Ueda, and D. K. Yamaguchi (2005). The Orphan Tsunami of 1700: Japanese clues to a parent earthquake in North America, *U.S. Geol. Surv. Profess. Pap. 1707,* University of Washington Press, Seattle, Washington.

Avnaim-Katav, S., W. R. Gehrels, L. N. Brown, E. Fard, and G. M. MacDonald (2017). Distributions of salt-marsh foraminifera along the coast of SW California, USA: Implications for sea-level reconstructions, *Mar. Micropaleontol.* **131,** 25–43.

Barlow, N. L. M., I. Shennan, A. J. Long, W. R. Gehrels, M. H. Saher, S. A. Woodroffe, and C. Hillier (2013). Salt marshes as late Holocene tide gauges, *Global Planet. Change* **106,** 90–110.

Birks, H. J. B. (1995). Quantitative palaeoenvironmental reconstructions, in *Statistical Modelling of Quaternary Science Data*, D. Maddy and J. S. Brew (Editors), Quaternary Research Association, Cambridge, United Kingdom, 161–254.

Briggs, R. W., S. E. Engelhart, A. R. Nelson, T. Dura, A. C. Kemp, P. J. Haeussler, D. R. Corbett, S. J. Angster, and L.-A. Bradley (2014). Uplift and subsidence reveal a nonpersistent megathrust rupture boundary (Sitkinak Island, Alaska), *Geophys. Res. Lett.* **41,** no. 7, 2289–2296.

Brooks, S., A. Gelman, G. Jones, and X.-L. Meng (2011). *Handbook of Markov Chain Monte Carlo*, CRC Press, Boca Raton, Florida.

Brudzinski, M. R., and R. M. Allen (2007). Segmentation in episodic tremor and slip all along Cascadia, *Geology* **35,** 907–910.

Cahill, N., A. C. Kemp, A. C. Parnell, and B. P. Horton (2016). A Bayesian hierarchical model for reconstructing relative sea level: From raw data to rates, *Clim. Past* **12,** 525–542.

Culver, S. J., and B. P. Horton (2005). Infaunal marsh foraminifera from the Outer Banks, North Carolina, USA, *J. Foraminifer. Res.* **35,** 148–170.

Darienzo, M. E., C. D. Peterson, and C. Clough (1994). Stratigraphic evidence for great subduction-zone earthquakes at four estuaries in northern Oregon, USA, *J. Coast. Res.* **10,** no. 4, 850–876.

DeMets, C., R. G. Gordon, and D. F. Argus (2010). Geologically current plate motions, *Geophys. J. Int.* **181,** 1–80.

Dura, T., S. E. Engelhart, M. Vacchi, B. P. Horton, R. E. Kopp, W. R. Peltier, and S. Bradley (2016). The role of Holocene relative sea-level change in preserving records of subduction zone earthquakes, *Curr. Clim. Change Rep.* **2,** 86–100.

Dura, T., E. Hemphill-Haley, Y. Sawai, and B. P. Horton (2016). The application of diatoms to reconstruct the history of subduction zone earthquakes and tsunamis, *Earth Sci. Rev.* **152,** 181–197.

Edwards, R. J., and A. J. Wright (2015). Foraminifera, in *Handbook of Sea-Level Research*, I. Shennan, A. J. Long, and B. P. Horton (Editors), John Wiley & Sons, Chichester, United Kingdom, 191–217.

Engelhart, S. E., B. P. Horton, A. R. Nelson, A. D. Hawkes, R. C. Witter, K. Wang, P.-L. Wang, and C. H. Vane (2013). Testing the use of microfossils to reconstruct great earthquakes at Cascadia, *Geology* **41,** 1067–1070.

Engelhart, S. E., B. P. Horton, C. H. Vane, A. R. Nelson, R. C. Witter, S. R. Brody, and A. D. Hawkes (2013). Modern foraminifera, $\delta^{13}C$, and bulk geochemistry of central Oregon tidal marshes and their application in paleoseismology, *Palaeogeogr. Palaeoclimatol. Palaeoecol.* **377,** 13–27.

Engelhart, S. E., M. Vacchi, B. P. Horton, A. R. Nelson, and R. E. Kopp (2015). A sea-level database for the Pacific coast of central North America, *Quaternary Sci. Rev.* **113,** 78–92.

Feng, L., E. M. Hill, P. Banerjee, I. Hermawan, L. L. H. Tsang, D. H. Natawidjaja, B. W. Suwargadi, and K. Sieh (2015). A unified GPS-based earthquake catalog for the Sumatran plate boundary between 2002 and 2013, *J. Geophys. Res.* **120,** 3566–3598.

Goldfinger, C., S. Galer, J. Beeson, T. Hamilton, B. Black, C. Romsos, J. Patton, C. H. Nelson, R. Hausmann, and A. Morey (2017). The importance of site selection, sediment supply, and hydrodynamics: A case study of submarine paleoseismology on the Northern Cascadia margin, Washington USA, *Mar. Geol.* **384,** 4–46.

Guilbault, J.-P., J. J. Clague, and M. Lapointe (1995). Amount of subsidence during a late Holocene earthquake—Evidence from fossil tidal marsh foraminifera at Vancouver Island, west coast of Canada, *Palaeogeogr. Palaeoclimatol. Palaeoecol.* **118,** 49–71.

Guilbault, J.-P., J. J. Clague, and M. Lapointe (1996). Foraminiferal evidence for the amount of coseismic subsidence during a late holocene earthquake on Vancouver Island, West Coast of Canada, *Quaternary Sci. Rev.* **15,** 913–937.

Hawkes, A. D., M. Bird, S. Cowie, C. Grundy-Warr, B. P. Horton, A. T. S. Hwai, L. Law, C. Macgregor, J. Nott, and J. E. Ong (2007). Sediments

deposited by the 2004 Indian Ocean tsunami along the Malaysia–Thailand Peninsula, *Mar. Geol.* **242,** 169–190.

Hawkes, A. D., B. P. Horton, A. R. Nelson, and D. F. Hill (2010). The application of intertidal foraminifera to reconstruct coastal subsidence during the giant Cascadia earthquake of AD 1700 in Oregon, USA, *Quaternary Int.* **221,** 116–140.

Hawkes, A. D., B. P. Horton, A. R. Nelson, C. H. Vane, and Y. Sawai (2011). Coastal subsidence in Oregon, USA, during the giant Cascadia earthquake of AD 1700, *Quaternary Sci. Rev.* **30,** 364–376.

Hemphill-Haley, E. (1995). Diatom evidence for earthquake-induced subsidence and tsunami 300 yr ago in southern coastal Washington, *Geol. Soc. Am. Bull.* **107,** 367–378.

Hill, M. O. (1973). Diversity and evenness: A unifying notation and its consequences, *Ecology* **54,** 427–432.

Holden, P. B., H. J. B. Birks, S. J. Brooks, M. B. Bush, G. M. Hwang, F. Matthews-Bird, B. G. Valencia, and R. van Woesik (2017). BUMPER v1.0: A Bayesian user-friendly model for palaeo-environmental reconstruction, *Geosci. Model Dev.* **10,** 483–498.

Horton, B. P. (1999). The distribution of contemporary intertidal foraminifera at Cowpen Marsh, Tees Estuary, UK: Implications for studies of Holocene sea-level changes, *Palaeogeogr. Palaeoclimatol. Palaeoecol.* **149,** 127–149.

Horton, B. P., and R. J. Edwards (2005). The application of local and regional transfer functions to the reconstruction of Holocene sea levels, north Norfolk, England, *Holocene* **15,** 216–228.

Horton, B. P., and R. J. Edwards (2006). *Quantifying Holocene Sea-Level Change Using Intertidal Foraminifera: Lessons from the British Isles*, Cushman Foundation for Foraminiferal Research, Washington, D.C.

Horton, B. P., Y. Milker, T. Dura, K. Wang, W. T. Bridgeland, L. Brophy, M. Ewald, N. S. Khan, S. E. Engelhart, A. R. Nelson, *et al.* (2017). Microfossil measures of rapid sea-level rise: Timing of response of two microfossil groups to a sudden tidal-flooding experiment in Cascadia, *Geology* **45,** no. 6, 535–538.

Hughes, J. F., R. W. Mathewes, and J. J. Clague (2002). Use of pollen and vascular plants to estimate coseismic subsidence at a tidal marsh near Tofino, British Columbia, *Palaeogeogr. Palaeoclimatol. Palaeoecol.* **185,** 145–161.

Hunger, A. A. (1966). Distribution of foraminifera, Netarts Bay, Oregon, *M.S. Thesis*, Department of Oceanography, Oregon State University, 123 pp.

Hutchinson, I., and J. Clague (2017). Were they all giants? Perspectives on late Holocene plate-boundary earthquakes at the northern end of the Cascadia subduction zone, *Quaternary Sci. Rev.* **169,** 29–49.

Jackson, S. T., and J. W. Williams (2004). Modern analogs in Quaternary paleoecology: Here today, gone yesterday, gone tomorrow?, *Ann. Rev. Earth Planet. Sci.* **32,** 495–537.

Jennings, A. E., and A. R. Nelson (1992). Foraminiferal assemblage zones in Oregon tidal marshes; relation to marsh floral zones and sea level, *J. Foraminifer. Res.* **22,** 13–29.

Jennings, A. E., A. R. Nelson, D. B. Scott, and J. C. Aravena (1995). Marsh foraminiferal assemblages in the Valdivia Estuary, south-central Chile, relative to vascular plants and sea level, *J. Coast. Res.* **11,** 107–123.

Juggins, S. (2011). *C2 Version 1.7.7*, available at https://www.staff.ncl.ac.uk/stephen.juggins/software/C2Home.htm (last accessed February 2018).

Juggins, S. (2013). Quantitative reconstructions in palaeolimnology: New paradigm or sick science?, *Quaternary Sci. Rev.* **64,** 20–32.

Juggins, S., and H. J. B. Birks (2012). Quantitative environmental reconstructions from biological data, in *Tracking Environmental Change Using Lake Sediments*, H. J. B. Birks, A. F. Lotter, S. Juggins, and J. P. Smol (Editors), Data Handling and Numerical Techniques, Springer, Dordrecht, The Netherlands, 431–494.

Kaufman, L., and P. J. Rousseeuw (2005). *Finding Groups in Data: An Introduction to Cluster Analysis*, Wiley-Interscience, Hoboken, New Jersey.

Kelsey, H. M., R. C. Witter, and E. Hemphill-Haley (2002). Plate-boundary earthquakes and tsunamis of the past 5500 yr, Sixes River estuary, southern Oregon, *Geol. Soc. Am. Bull.* **114,** 298–314.

Kemp, A. C., and R. J. Telford (2015). Transfer functions, in *Handbook for Sea-Level Research*, I. Shennan, A. J. Long, and B. P. Horton (Editors), John Wiley & Sons, Chichester, United Kingdom, 470–499.

Kemp, A. C., M. A. Buzas, S. J. Culver, and B. P. Horton (2011). Influence of patchiness on modern salt-marsh foraminifera used in sea-level studies (North Carolina, USA), *J. Foraminifer. Res.* **41,** 114–123.

Kenkel, N. C., and L. Orlóci (1986). Applying metric and nonmetric multidimensional scaling to ecological studies: Some new results, *Ecology* **67,** 919–928.

Kruskal, J. B. (1964). Multidimensional scaling by optimizing goodness of fit to a nonmetric hypothesis, *Psychometrika* **29,** 1–27.

Lang, S., and A. Brezger (2004). Bayesian P-splines, *J. Comput. Graph. Stat.* **13,** 183–212.

Leonard, L. J., C. A. Currie, S. Mazzotti, and R. D. Hyndman (2010). Rupture area and displacement of past Cascadia great earthquakes from coastal coseismic subsidence, *Geol. Soc. Am. Bull.* **122,** 2079–2096.

Leonard, L. J., R. D. Hyndman, and S. Mazzotti (2004). Coseismic subsidence in the 1700 great Cascadia earthquake: Coastal estimates versus elastic dislocation models, *Geol. Soc. Am. Bull.* **116,** 655–670.

Mamo, B., L. Strotz, and D. Dominey-Howes (2009). Tsunami sediments and their foraminiferal assemblages, *Earth Sci. Rev.* **96,** 263–278.

Manske, D. C. (1968). Distribution of recent foraminifera in relation to estuarine hydrography, Yaquina Bay, Oregon, *Ph.D. Thesis*, Department of Oceanography, Oregon State University.

McCaffrey, R., R. W. King, S. J. Payne, and M. Lancaster (2013). Active tectonics of northwestern U.S. inferred from GPS-derived surface velocities, *J. Geophys. Res.* **118,** 709–723.

Milker, Y., B. P. Horton, A. R. Nelson, S. E. Engelhart, and R. C. Witter (2015). Variability of intertidal foraminiferal assemblages in a salt marsh, Oregon, USA, *Mar. Micropaleontol.* **118,** 1–16.

Milker, Y., A. R. Nelson, B. P. Horton, S. E. Engelhart, L.-A. Bradley, and R. C. Witter (2016). Differences in coastal subsidence in southern Oregon (USA) during at least six prehistoric megathrust earthquakes, *Quaternary Sci. Rev.* **142,** 143–163.

Murray, J. W. (2006). *Ecology and Applications of Benthic Foraminifera*, Cambridge University Press, Cambridge, United Kingdom.

Nelson, A. R. (1992). Discordant ^{14}C ages from buried tidal-marsh soils in the Cascadia subduction zone, southern Oregon coast, *Quaternary Res.* **38,** 74–90.

Nelson, A. R. (2013). Tectonics and relative sea-level change, in *Encyclopedia of Quaternary Science*, Second Ed., A. E. Scott (Editor-in-Chief), Elsevier, Amsterdam, The Netherlands, 503–519.

Nelson, A. R., and K. Kashima (1993). Diatom zonation in southern Oregon tidal marshes relative to vascular plants, foraminifera, and sea level, *J. Coast. Res.* **9,** no. 3, 673–697.

Nelson, A. R., and S. F. Personius (1996). Great-earthquake potential in Oregon and Washington: An overview of recent coastal geologic studies and their bearing on segmentation of Holocene ruptures, central Cascadia subduction zone, *U.S. Geol. Surv. Profess. Pap.*, 91–114.

Nelson, A. R., H. M. Kelsey, and R. C. Witter (2006). Great earthquakes of variable magnitude at the Cascadia subduction zone, *Quaternary Res.* **65,** 354–365.

Nelson, A. R., Y. Sawai, A. E. Jennings, L.-A. Bradley, L. Gerson, B. L. Sherrod, J. Sabean, and B. P. Horton (2008). Great-earthquake paleogeodesy and tsunamis of the past 2000 years at Alsea Bay, central Oregon coast, USA, *Quaternary Sci. Rev.* **27,** 747–768.

Nelson, A. R., I. Shennan, and A. J. Long (1996). Identifying coseismic subsidence in tidal-wetland stratigraphic sequences at the Cascadia subduction zone of western North America, *J. Geophys. Res.* **101,** 6115–6135.

Patterson, R. T., J.-P. Guilbault, and J. J. Clague (1999). Taphonomy of tidal marsh foraminifera: Implications of surface sample thickness for high-resolution sea-level studies, *Palaeogeogr. Palaeoclimatol. Palaeoecol.* **149,** 199–211.

Peterson, C. D., D. L. Doyle, and E. T. Barnett (2000). Coastal flooding and beach retreat from coseismic subsidence in the central Cascadia margin, USA, *Environ. Eng. Geosci.* **6,** 255–269.

Pilarczyk, J. E., B. P. Horton, R. C. Witter, C. H. Vane, C. Chagué-Goff, and J. Goff (2012). Sedimentary and foraminiferal evidence of the 2011 Tōhoku-oki tsunami on the Sendai coastal plain, Japan, *Sediment. Geol.* **282,** 78–89.

Redfield, A. C. (1965). Ontogeny of a salt marsh estuary, *Science* **147,** 50–55.

Rousseeuw, P. (1987). Silhouettes: A graphical aid to the interpretation and validation of cluster techniques, *J. Comput. Appl. Math.* **20,** 53–65.

Sabean, J. (2004). Application of foraminifera to detecting land level change associated with great earthquakes along the west coast of North America, *M.Sc. Thesis*, Department of Earth Sciences, Simon Fraser University, 85 pp.

Sachs, H. M., T. Webb, and D. R. Clark (1977). Paleoecological transfer functions, *Ann. Rev. Earth Planet. Sci.* **5,** 159–178.

Sawai, Y., B. P. Horton, A. C. Kemp, A. D. Hawkes, T. Nagumo, and A. R. Nelson (2016). Relations between diatoms and tidal environments in Oregon and Washington, USA, *Diatom Res.* **31,** no. 1, 17–38.

Schmalzle, G. M., R. McCaffrey, and K. C. Creager (2014). Central Cascadia subduction zone creep, *Geochem. Geophys. Geosys.* **15,** 1515–1532.

Scott, D. B., and F. S. Medioli (1978). Vertical zonations of marsh foraminifera as accurate indicators of former sea levels, *Nature* **272,** 528–531.

Scott, D. B., E. S. Collins, J. Duggan, A. Asioli, T. Saito, and S. Hasegawa (1996). Pacific rim marsh foraminiferal distributions: Implications for sea-level studies, *J. Coast. Res.* **12,** 850–861.

Scott, D. K., and R. M. Leckie (1990). Foraminiferal zonation of Great Sippewissett salt marsh (Falmouth, Massachusetts), *J. Foraminifer. Res.* **20,** 248–266.

Seliskar, D. M., and J. L. Gallagher (1983). *Ecology of Tidal Marshes of the Pacific Northwest Coast: A Community Profile*, U.S. Fish and Wildlife Service, 65 pp.

Shennan, I., E. Garrett, and N. Barlow (2016). Detection limits of tidal-wetland sequences to identify variable rupture modes of megathrust earthquakes, *Quaternary Sci. Rev.* **150,** 1–30.

Shennan, I., A. Long, M. Rutherford, F. Green, J. Innes, J. Lloyd, Y. Zong, and K. Walker (1996). Tidal marsh stratigraphy, sea-level change and large earthquakes, I: A 5000 year record in Washington, USA, *Quaternary Sci. Rev.* **15,** 1023–1059.

Simpson, G. L. (2012). Analogue methods, in *Data Handling and Numerical Techniques*, H. J. B. Birks, A. F. Lotter, S. Juggins, and J. P. Smol (Editors), Springer, Dordrecht, The Netherlands, 495–522.

Tréhu, A. M., R. J. Blakely, and M. C. Williams (2012). Subducted seamounts and recent earthquakes beneath the central Cascadia forearc, *Geology* **40,** 103–106.

Tréhu, A. M., J. Braunmiller, and E. Davis (2015). Seismicity of the central Cascadia continental margin near 44.5° N: A decadal view, *Seismol. Res. Lett.* **86,** 819–829.

Wang, K., and S. L. Bilek (2011). Do subducting seamounts generate or stop large earthquakes?, *Geology* **39,** 819–822.

Wang, K., and A. M. Tréhu (2016). Invited review paper: Some outstanding issues in the study of great megathrust earthquakes—The Cascadia example, *J. Geodyn.* **98,** 1–18.

Wang, K., Y. Hu, and J. He (2012). Deformation cycles of subduction earthquakes in a viscoelastic Earth, *Nature* **484,** 327–332.

Wang, P.-L., S. E. Engelhart, K. Wang, A. D. Hawkes, B. P. Horton, A. R. Nelson, and R. C. Witter (2013). Heterogeneous rupture in the great Cascadia earthquake of 1700 inferred from coastal subsidence estimates, *J. Geophys. Res.* **118,** 2460–2473.

Watcham, E. P., I. Shennan, and N. L. M. Barlow (2013). Scale considerations in using diatoms as indicators of sea-level change: Lessons from Alaska, *J. Quaternary Sci.* **28,** 165–179.

Wells, R. E., R. J. Blakely, Y. Sugiyama, D. W. Scholl, and P. A. Dinterman (2003). Basin-centered asperities in great subduction zone earthquakes: A link between slip, subsidence, and subduction erosion?, *J. Geophys. Res.* **108,** 2507, doi: 10.1029/2002JB002072.

Witter, R. C., H. M. Kelsey, and E. Hemphill-Haley (2003). Great Cascadia earthquakes and tsunamis of the past 6700 years, Coquille River estuary, southern coastal Oregon, *Geol. Soc. Am. Bull.* **115,** 1289–1306.

Wright, A. J., R. J. Edwards, and O. van de Plassche (2011). Reassessing transfer-function performance in sea-level reconstruction based on benthic salt-marsh foraminifera from the Atlantic coast of NE North America, *Mar. Micropaleontol.* **81,** 43–62.

Department of Earth and Ocean Sciences
Tufts University
2 North Hill Road
Medford, Massachusetts 02155
andrew.kemp@tufts.edu
(A.C.K.)

School of Mathematics and Statistics
University College Dublin
Science Center North
Belfield, Dublin 4
Ireland
(N.C.)

Department of Geosciences
University of Rhode Island
9 E. Alumni Avenue
Kingston, Rhode Island 02881
(S.E.E.)

Department of Earth and Ocean Sciences
University of North Carolina Wilmington
601 South College Road
Wilmington, North Carolina 28403
(A.D.H.)

Pacific Geoscience Centre
Geological Survey of Canada
Natural Resources Canada
Sidney, British Columbia
Canada V8L 4B2
(K.W.)